Coupled cluster valence bond theory for open-shell systems with application to very long range strong correlation in a polycarbene dimer

David W. Small and Martin Head-Gordon

Department of Chemistry, University of California, Berkeley, California 94720, USA and Chemical Sciences Division, Lawrence Berkeley National Laboratory, Berkeley, California 94720, USA

(Dated: June 23, 2017)

Abstract

The Coupled Cluster Valence Bond (CCVB) method, previously presented for closed-shell (CS) systems, is extended to open-shell (OS) systems. The theoretical development is based on embedding the basic OS CCVB wave function in a fictitious singlet super-system. This approach reveals that the OS CCVB amplitude equations are quite similar to those of CS CCVB, and thus that OS CCVB requires the same level of computational effort as CS CCVB, which is an inexpensive method. We present qualitatively correct CCVB potential energy curves for all low-lying spin states of P_2 and Mn_2^+. CCVB is successfully applied to the low-lying spin states of some model linear polycarbenes, systems that appear to be a hinderance to standard density functionals. We examine an octa-carbene dimer in a side-by-side orientation, which, in the monomer dissociation limit, exhibits maximal strong correlation over the length of the polycarbene.

I. INTRODUCTION

The most widely used methods in electronic structure theory are based on a single determinant of molecular orbitals (MOs). Most prominently, Kohn-Sham density functional theory (DFT),[1,2] uses a reference determinant that describes non-interacting electrons with the same density, $\rho(\mathbf{r})$, as the physical system of interest. The task of the exchange-correlation functional (XCF) is to describe non-classical electron-electron interactions. Computationally efficient XCFs use one-point density gradient and/or kinetic energy density corrections to the local density approximation (LDA) that work well when key correlation effects are atomic-like (i.e. spatially localized). Two-point corrections for weak long-range dispersion effects are becoming widely used.[3–5] However, present-day XCFs break down when strong correlation effects are present.[6] Widely used wavefunction methods such as coupled cluster (CC) theory[7] and Møller-Plesset (MP) perturbation theory[8] also correct a single determinant reference for the effects of electron-electron correlations. CC theory is exact if no truncation is made in the cluster expansion, but in practice is typically truncated at single and double (SD) or triple substitutions (T) to retain acceptable computational efficiency. The workhorse CCSD(T) method[9] yields high accuracy for problems where the single determinant is an acceptable single reference. Similarly low-order MP theory such as MP2, MP3, MP4, etc, is also useful in this regime.

Strong correlations, the main topic of this paper, may be diagnosed by poor performance of low-order MP theory.[10] A standard example is the "recoupling region" in chemical bond-breaking,[10] which are displacements beyond the Coulson-Fischer point of spin-polarization onset, and before the dissociation limit is approached. Other examples include the spin-recoupling of transition metals[11] and emergent strong correlations in systems such as larger oligoacenes.[12,13] Present-day XCFs in DFT likewise usually perform poorly for strongly correlated systems. Strongly correlated systems often are associated with multiple low-lying electronic states of differing spin. For instance, in bond dissociations, low-spin coupling (e.g. the singlet state of N_2) becomes degenerate with high-spin coupling (the heptet state associated with 2 quartet N atoms) in the dissociation limit. Therefore it is seldom enough to evaluate just a single spin state in systems where strong correlations are in play. Rather, it is desirable to be able to examine (at least) the ground state for all members of the spin manifold. That will be our purpose in this paper.

If not too many electrons are strongly entangled, the most widely used alternative to the mean field reference is a complete active space SCF (CASSCF) reference. CASSCF is the exact solution of the Schrödinger equation in a variationally optimized set of active orbitals,[14–21] with some inactive mean-field orbitals that are weakly correlated, and only as many virtual orbitals as needed to describe the strong correlations. One logical extreme for the active space is the full valence set, which is equal in number to the sum of valence atomic orbitals (AOs) on all atoms. Full valence CASSCF can exactly separate any molecule into its constituent atoms (in the sense of yielding the sum of atomic CASSCF energies). Fewer active orbitals are often used by computational necessity, because the formal scaling of CASSCF is exponential in active space size. Advances in numerical methods[22–24] are helping to improve the efficiency of CASSCF calculations in large active spaces. There has also been significant effort to develop systematic truncations of the CASSCF problem, using either (non-size-consistent) CI approaches[25,26] or (size-consistent) CC approaches.[27–31] Reduced density matrix (RDM) solvers for the CASSCF problem also have shown promising results.[32–34]

While less widely used, spin-coupled valence bond (SCVB) theory[35–37] is another alternative reference that is conceptually appealing because it represents the ultimate single particle model. The spatial part of the SCVB wavefunction is a simple product of orbitals, one for each electron. No constraints are placed on the orbitals (i.e. they are non-orthogonal). Some electron pairs may be inactive, as in CASSCF. The spin part of the SCVB wavefunction couples the spatial orbitals in every possible way to obtain a state with the target total spin and its z component. As a result, SCVB can correctly separate a molecule into its constituent atoms, representing a key class of strong correlations. SCVB is often a very good approximation to CASSCF, and there exist extensions of SCVB for when this is not the case; see ref.s 38 and 39 for two recent interesting examples. The number of SCVB spin couplings rises exponentially with number of active electrons, which, together with the non-orthogonality of the spatial orbitals, poses a formidable computational challenge.

That computational challenge invites the question of how SCVB can be efficiently approximated without losing its ability to treat important classes of strong correlations. The most drastic approximation is to consider correlations only within a pair of electrons, as occurs in separating isolated single bonds into radical fragments, while inter-pair interactions are treated by mean field (as are any unpaired electrons). Orbitals in different pairs

are also assumed to be orthogonal.[40] This perfect pairing (PP) model retains the conceptual VB picture (indeed, it is often called generalized VB (GVB),[41]) giving localized orbitals that correspond to bonds and antibonds, but can be efficiently implemented.[42,43] PP is the simplest geminal[44] (i.e. 2-particle building blocks) approach to electronic structure. There are also numerous more sophisticated geminal theories.[45–53]

The essential limitation of PP is its inability to correctly treat two or more pairs of strongly entangled electrons. For instance in the separation of ethene:

$$C_2H_4\left(^1A_1\right) \longrightarrow 2CH_2\left(^3B_1\right) \tag{1}$$

PP cannot achieve the correct dissociation limit. While it describes the separation of two isolated bonds correctly, two bonds in the same spatial region breaking together involves correlations between the electrons in the two relevant electron pairs. In other words, there is strong inter-geminal coupling in double bond-breaking, and the same is true whenever there are more than two strongly correlated electrons in the same spatial region. CI-based corrections such as the GVB-RCI hierarchy[54,55] were developed to account for interpair coupling, followed later by CC-based approaches.[56–58] The latter have been extended to high order methods such as perfect quadruples (PQ)[29,31] and hextuples (PH).[30,31] The goal of proceeding to more sophisticated theories that incorporate geminal coupling[53] is an important research direction that bridges the gap between independent geminal theories and either SCVB or CASSCF.

Our present focus is on (what may be) the simplest useful approach that can correct the main deficiencies of PP for multiple bond-breaking, while not increasing the computational cost unreasonably. This approach is the coupled cluster valence bond (CCVB) method,[10,59] which takes the PP wavefunction as its reference, and corrects it with a coupled-cluster-like expansion whose variables are pair-pair recoupling amplitudes. This method was inspired by the form of the projected unrestricted HF (PUHF) wave function. Adopting this wavefunction ansatz and determining the amplitudes projectively allows the CCVB method to be size-consistent and to agree with SCVB and CASSCF at the dissociation limit (in the corresponding active spaces). The simplicity of the CCVB wavefunction also permits efficient implementation, which we have described in detail.[60]

CCVB has demonstrated good agreement with CASSCF for problems in which strong spin correlations are at play, such as bond-breaking,[10,59] while, like PP,[61] its link to a single Lewis

structure causes difficulties such as symmetry breaking and multiple solutions in orbital optimization in systems where multiple resonance structures contribute on an equal or nearly equal footing.[10] These difficulties can be reduced or eliminated at additional computational cost by using a generalization of CCVB, termed CCVB-SD, that subsumes the PP-based pairing structure of CCVB into full inclusion of all single and double substitutions,[62] in analogy to the standard CCSD method. The quadratic number of amplitudes in CCVB are then replaced by the full quartic number of singles and doubles in CCVB-SD. An efficient implementation of CCVB-SD for closed shell systems has recently been reported,[63] enabling the treatment of large acenes, which are problematical using CCVB itself.[60]

This paper addresses the issue raised in the second paragraph of this Introduction regarding open shell (non-singlet) systems with strong correlations. Such systems will typically have low-lying states of different spin multiplicities because the strongly entangled electrons are not strongly coupled into pairs. Therefore it is highly desirable to extend the basic CCVB method from its previously reported closed shell theory and implementation to open shell states of molecules with either even or odd numbers of electrons. In Sec. II, CCVB is extended to permit treatment of any number of excess electrons of α spin. The open shell formalism is first developed explicitly (Sec. II A), then recast into a pseudo closed-shell form, using fictitious non-interacting orbitals (and electrons) (Sec. II B), which finally forms a basis for efficient implementation as a modification of the closed shell CCVB method (Sec. II C). A variety of computational applications are reported in Sec. III to assess the performance of OS-CCVB, beginning with the singlet, triplet, quintet and heptet states of P_2, and the spin states $s = \frac{1}{2}$ through $s = \frac{11}{2}$ of Mn_2^+, which is a very interesting ion because the ground state is ferromagnetic.

The main application in Sec. III is to spin states of model oligocarbenes. Methylene, the simplest carbene has about a 0.4 eV preference for triplet $s = 1$ relative to singlet $s = 0$. Low energy states of dicarbenes then arise from the different ways ($s = 0, s = 1, s = 2$) in which two $s = 1$ sites can recouple. Depending on the organic linkers connecting the carbenes, any of the three states may be the ground state. There has been considerable experimental and computational interest in dicarbenes, as one of several possible building blocks towards larger organic molecules that might support high spin states.[64,65] For instance, bridging phenyl groups promote a ferromagnetic ground state, which is well described by a single determinant. Any other spin state of a dicarbene or higher represents a strongly correlated system.

There have been several computational studies of poly(m-phenylenecarbene) systems.[66,67] Here, using methylene linkers for simplicity, we report benchmark assessments of OS-CCVB for di- and tetra- carbenes. Octa-carbene calculations turn out to pose substantial challenges for OS-CCVB calculations, which we discuss. These difficulties are circumvented in our final example by considering a dimer of octa-carbene, which is viable with OS-CCVB. At larger separations, this system turns out to exhibit extraordinary non-locality of strong electron correlations, which makes it very interesting in its own right.

II. THEORY

Much of what follows is rooted in the developments of the previous CCVB papers.[59,60] We assume an open-shell system with n_α α-spin electrons and n_β β-spin electrons. We define $n_x = n_\alpha - n_\beta$, the number of "excess" α-spin electrons. Below, we give a detailed derivation of our approach to OS CCVB. The end result is that OS CCVB is obtained as a relatively straightforward modification to CS CCVB. Readers interested primarily in this result may wish to skip ahead to Section II C.

A. CCVB configurations and the OS CCVB wave function

One of the principles of CCVB is a partition of the electrons into pairs. For an OS system, we have n_β pairs, which will be numbered 1 through n_β and, more abstractly, indexed by the letters $k, l, m, \ldots$, i.e. in what follows we assume the convention

$$1 \leq k, l, m, n \leq n_\beta. \tag{2}$$

Similarly, we will associate the OS electrons and related entities with the numbers $n_\beta + 1$ through $n_\beta + n_x$.

Each pair is treated as 2 electrons in 2 orbitals, and for this, we work with two orthonormal spatial orbitals, ϕ_k and $\phi_{\hat{k}}$. These give rise to four orthonormal spin orbitals, which will be represented by their second-quantization counterparts $\mathbf{a}^\dagger_{k_\alpha}$, $\mathbf{a}^\dagger_{\hat{k}_\alpha}$, $\mathbf{a}^\dagger_{k_\beta}$, and $\mathbf{a}^\dagger_{\hat{k}_\beta}$. The set containing all orbitals from all pairs is constrained to be orthonormal.

For each pair, we construct geminals

$$\mathbf{g}^\dagger_{\mathbf{s},k} = \frac{1}{\sqrt{2(1+\cos^2(\theta_k))}} \left(2\cos(\theta_k)\, \mathbf{a}^\dagger_{k_\alpha} \mathbf{a}^\dagger_{k_\beta} - \sin(\theta_k)\, \mathbf{a}^\dagger_{k_\alpha} \mathbf{a}^\dagger_{\hat{k}_\beta} - \sin(\theta_k)\, \mathbf{a}^\dagger_{\hat{k}_\alpha} \mathbf{a}^\dagger_{k_\beta} \right), \tag{3}$$

where θ_k is a parameter, and

$$\begin{aligned}
\mathbf{g}^\dagger_{\mathbf{t_1},k} &= \frac{1}{\sqrt{2}}(-\mathbf{a}^\dagger_{k_\alpha}\mathbf{a}^\dagger_{\hat{k}_\beta} + \mathbf{a}^\dagger_{\hat{k}_\alpha}\mathbf{a}^\dagger_{k_\beta}) \\
\mathbf{g}^\dagger_{\mathbf{t_2},k} &= \mathbf{a}^\dagger_{k_\alpha}\mathbf{a}^\dagger_{\hat{k}_\alpha} \\
\mathbf{g}^\dagger_{\mathbf{t_3},k} &= \mathbf{a}^\dagger_{k_\beta}\mathbf{a}^\dagger_{\hat{k}_\beta}.
\end{aligned} \tag{4}$$

Since the orbitals are fully orthonormal, geminals for different pairs are "strongly orthogonal" to each other. This helps tremendously in the computation of Hamiltonian matrix elements.[59] As with other correlation approximations, CCVB utilizes the concept of active spaces. In practice, the first several pairs may be chosen to be "inactive", and are treated as they would be in Restricted Hartree Fock (RHF). For each of these pairs, the above triplet geminal operators are irrelevant, while the singlet geminal operator is defined simply to be $\mathbf{a}^\dagger_{k_\alpha}\mathbf{a}^\dagger_{k_\beta}$.[60]

To each OS electron we associate a spatial orbital, which has counterpart second quantization operators $\mathbf{a}^\dagger_{\kappa_\alpha}$ and $\mathbf{a}^\dagger_{\kappa_\beta}$. In general we will label OS entities with Greek letters $\kappa, \lambda, \mu, \ldots$, i.e.

$$n_\beta + 1 \leq \kappa, \lambda, \mu, \nu \leq n_\beta + n_x. \tag{5}$$

We will use indices $a, b, c, \ldots$ for the more general case when CS or OS has not been specified, i.e.

$$1 \leq a, b, c, d \leq n_\beta + n_x. \tag{6}$$

The OS orbitals are constrained to be fully orthonormal among themselves and to the pair-based orbitals.

Grouping all the annihilation operators corresponding to all the above orbitals, i.e. the pair-based ones and the OS ones, into a set $\mathcal{Q}_m$, we obtain a Hamiltonian operator $\mathbf{H}_m = \hat{H}(\mathcal{Q}_m)$, where, more generally,

$$\hat{H}(\mathcal{X}) = \sum_{\mathbf{a}_w, \mathbf{a}_x \in \mathcal{X}} \langle 0|\mathbf{a}_w\, \hat{h}\, \mathbf{a}^\dagger_x|0\rangle\, \mathbf{a}^\dagger_w \mathbf{a}_x + \frac{1}{4} \sum_{\mathbf{a}_w, \mathbf{a}_x, \mathbf{a}_y, \mathbf{a}_z \in \mathcal{X}} \langle 0|\mathbf{a}_x \mathbf{a}_w\, \hat{V}\, \mathbf{a}^\dagger_y \mathbf{a}^\dagger_z|0\rangle\, \mathbf{a}^\dagger_w \mathbf{a}^\dagger_x \mathbf{a}_z \mathbf{a}_y, \tag{7}$$

where $|0\rangle$ is the vacuum state, $\hat{h}$ is the sum of the kinetic energy and nuclear attraction operators, and $\hat{V}$ is the Coulomb operator.

A blueprint for OS CCVB was given in the original CCVB paper,[59] so we will give only an overview here. The OS CCVB wave function $|\boldsymbol{\psi}\rangle$ is a linear combination of various

substituted configurations. The first of these is the reference configuration, which is a natural extension of that for the CS case:

$$|\boldsymbol{\psi}_0\rangle = \left(\prod_{k=1}^{n_\beta} \mathbf{g}^\dagger_{\mathbf{s},k}\right)\left(\prod_{\kappa=n_\beta+1}^{n_\beta+n_x} \mathbf{a}^\dagger_{\kappa_\alpha}\right)|0\rangle. \tag{8}$$

$|\boldsymbol{\psi}_0\rangle$ is basically an open-shell Perfect Pairing wavefunction. The remaining configurations used to define $|\boldsymbol{\psi}\rangle$ are obtained by making certain substitutions in the reference. For the CS part of the reference, we have all the same substitutions we would have in the CS case. The simplest of these are the configurations that substitute two singlet pairs, $|\boldsymbol{\psi}_{(kl)}\rangle$. These are obtained by making the following replacement in the reference.

$$\mathbf{g}^\dagger_{\mathbf{s},k}\mathbf{g}^\dagger_{\mathbf{s},l} \;\rightarrow\; \mathbf{d}^\dagger_{\mathbf{s_2},kl} = \frac{1}{\sqrt{3}}\big(\mathbf{g}^\dagger_{\mathbf{t_1},k}\mathbf{g}^\dagger_{\mathbf{t_1},l} - \mathbf{g}^\dagger_{\mathbf{t_2},k}\mathbf{g}^\dagger_{\mathbf{t_3},l} - \mathbf{g}^\dagger_{\mathbf{t_3},k}\mathbf{g}^\dagger_{\mathbf{t_2},l}\big). \tag{9}$$

There are also configurations $|\boldsymbol{\psi}_{(klm)}\rangle$ in which 3 singlet pairs have been substituted:

$$\mathbf{g}^\dagger_{\mathbf{s},k}\mathbf{g}^\dagger_{\mathbf{s},l}\mathbf{g}^\dagger_{\mathbf{s},m} \;\rightarrow\; \mathbf{e}^\dagger_{\mathbf{s_5},klm}, \tag{10}$$

where

$$\begin{aligned}\mathbf{e}^\dagger_{\mathbf{s_5},klm} = \frac{1}{\sqrt{6}}\Big(&\mathbf{g}^\dagger_{\mathbf{t_1},k}(\mathbf{g}^\dagger_{\mathbf{t_2},l}\mathbf{g}^\dagger_{\mathbf{t_3},m} - \mathbf{g}^\dagger_{\mathbf{t_3},l}\mathbf{g}^\dagger_{\mathbf{t_2},m}) \\ &-\mathbf{g}^\dagger_{\mathbf{t_2},k}\mathbf{g}^\dagger_{\mathbf{t_1},l}\mathbf{g}^\dagger_{\mathbf{t_3},m} + \mathbf{g}^\dagger_{\mathbf{t_3},k}\mathbf{g}^\dagger_{\mathbf{t_1},l}\mathbf{g}^\dagger_{\mathbf{t_2},m} \\ &+(\mathbf{g}^\dagger_{\mathbf{t_2},k}\mathbf{g}^\dagger_{\mathbf{t_3},l} - \mathbf{g}^\dagger_{\mathbf{t_3},k}\mathbf{g}^\dagger_{\mathbf{t_2},l})\mathbf{g}^\dagger_{\mathbf{t_1},m}\Big).\end{aligned} \tag{11}$$

We also make substitutions involving the open-shell part of the reference. The simplest of these configurations are denoted by $|\boldsymbol{\psi}_{(k\lambda)}\rangle$, where we have jointly replaced one singlet pair and one OS orbital in the reference:

$$\mathbf{g}^\dagger_{\mathbf{s},k}\mathbf{a}^\dagger_{\lambda_\alpha} \;\rightarrow\; \mathbf{d}^\dagger_{\mathbf{d_2},k\lambda} = \frac{1}{\sqrt{3}}\left(\mathbf{g}^\dagger_{\mathbf{t_1},k}\mathbf{a}^\dagger_{\lambda_\alpha} + \sqrt{2}\,\mathbf{g}^\dagger_{\mathbf{t_2},k}\mathbf{a}^\dagger_{\lambda_\beta}\right). \tag{12}$$

This is an analogue of eq. (9).

There is one remaining primary open-shell substitution, wherein we jointly replace 2 singlet pairs and one OS orbital in the reference:

$$\mathbf{g}^\dagger_{\mathbf{s},k}\mathbf{g}^\dagger_{\mathbf{s},l}\mathbf{a}^\dagger_{\mu_\alpha} \;\rightarrow\; \mathbf{e}^\dagger_{\mathbf{d_5},kl\mu}, \tag{13}$$

where

$$\begin{aligned}\mathbf{e}^\dagger_{\mathbf{d_5},kl\mu} = \frac{1}{\sqrt{6}}\Big(&-\sqrt{2}(\mathbf{g}^\dagger_{\mathbf{t_1},k}\mathbf{g}^\dagger_{\mathbf{t_2},l} - \mathbf{g}^\dagger_{\mathbf{t_2},k}\mathbf{g}^\dagger_{\mathbf{t_1},l})\mathbf{a}^\dagger_{\mu_\beta} \\ &+ (\mathbf{g}^\dagger_{\mathbf{t_2},k}\mathbf{g}^\dagger_{\mathbf{t_3},l} - \mathbf{g}^\dagger_{\mathbf{t_3},k}\mathbf{g}^\dagger_{\mathbf{t_2},l})\mathbf{a}^\dagger_{\mu_\alpha}\Big).\end{aligned} \tag{14}$$

This produces the configuration $|\boldsymbol{\psi}_{(kl\mu)}\rangle$.

The remaining configurations are obtained by repeated application of the substitutions described above in eqs. (9), (10), (12), and (13). The key for this is to not repeat any indices if there are multiple substitutions. We obtain configurations like $|\boldsymbol{\psi}_{(kl)(m\kappa)}\rangle$, $|\boldsymbol{\psi}_{(k\lambda)(l\mu)}\rangle$, $|\boldsymbol{\psi}_{(kl)(mn)(op)(q\kappa)}\rangle$, $|\boldsymbol{\psi}_{(kl)(mn)(o\kappa)(p\lambda)}\rangle$, $|\boldsymbol{\psi}_{(kl)(m\kappa)(n\lambda)(o\mu)}\rangle$, $|\boldsymbol{\psi}_{(k\kappa)(l\lambda)(m\mu)(n\nu)}\rangle$, etc. The full set of configurations obtained in this way will be called the "$\boldsymbol{\psi}$" set.

We can now describe the OS CCVB wave function. We normalize to the reference

$$\langle\boldsymbol{\psi}_0|\boldsymbol{\psi}\rangle = 1 \tag{15}$$

and define amplitudes

$$t_{ka} = \langle\boldsymbol{\psi}_{(ka)}|\boldsymbol{\psi}\rangle. \tag{16}$$

The 3-index configurations do not contribute:

$$\langle\boldsymbol{\psi}_{(kla)}|\boldsymbol{\psi}\rangle = 0, \tag{17}$$

while

$$\langle\boldsymbol{\psi}_{(ka)(lb)}|\boldsymbol{\psi}\rangle = t_{ka}t_{lb}, \tag{18}$$

and so on for higher-order substitutions. The latter equation demonstrates the coupled-cluster nature of the wave function.

In the usual way, we treat the amplitudes as variables. Collecting them into a vector $\mathbf{t}$, they can, in principle, be computed by solving $\xi_{ka}(\mathbf{t}) = 0$, where

$$\xi_{ka}(\mathbf{t}) = \langle\boldsymbol{\psi}_{(ka)}|\mathbf{H}_m|\boldsymbol{\psi}\rangle - t_{ka}\boldsymbol{\epsilon} \tag{19}$$

and

$$\boldsymbol{\epsilon} = \langle\boldsymbol{\psi}_0|\mathbf{H}_m|\boldsymbol{\psi}\rangle. \tag{20}$$

There is a difficulty here, however. To make these equations practicable, we need to have $|\boldsymbol{\psi}\rangle$'s expansion coefficients relative to the $\boldsymbol{\psi}$-set configurations. While the above overlaps of these configurations with $|\boldsymbol{\psi}\rangle$ do fully specify the latter, they do not directly provide the desired expansion coefficients. Rather, they directly provide the expansion coefficients relative to the configurations of what is known as the "dual set" of the $\boldsymbol{\psi}$ set. This point is nontrivial in the current setting because the $\boldsymbol{\psi}$ set is not orthogonal - indeed it is usually

linearly dependent - so it does not equal its dual set. The configurations of the latter are implicitly given by

$$|\boldsymbol{\phi}_i\rangle = \sum_j S^{-1}_{ji}|\boldsymbol{\psi}_j\rangle, \tag{21}$$

where S is the overlap matrix for the $\boldsymbol{\psi}$ set and we are using the Moore-Penrose pseudoinverse. Since the $\boldsymbol{\psi}$ set and its dual are in one-to-one correspondence, we use the same indexing scheme in each. The dual set will also be called the "$\boldsymbol{\phi}$" set. We emphasize that with the above definition of cluster amplitudes, t_{ka} corresponds directly to $|\boldsymbol{\phi}_{(ka)}\rangle$, not $|\boldsymbol{\psi}_{(ka)}\rangle$, these two configurations being unequal if the system has more than one unpaired electron.

The degree of difficulty of working with the inverse of S determines that for obtaining the expansion coefficients relative to the $\boldsymbol{\psi}$ set. The basic configurations of CS CCVB also form a nonorthogonal set, but its S, or, more precisely, the part of its S that is required for the CS CCVB amplitude equations, is sparse enough to be quite manageable. This is not the case for the OS S. For example, $\langle\boldsymbol{\psi}_{(k\mu)}|\boldsymbol{\psi}_{(k\nu)}\rangle \neq 0$ even if $\mu \neq \nu$, whereas the 2-pair substituted configurations in the CS case form an orthonormal set, and $\langle\boldsymbol{\psi}_{(kl)}|\boldsymbol{\psi}_{(k\mu)(l\nu)}\rangle \neq 0$, whereas configurations with different substitution levels are always orthogonal in CS CCVB. The higher the level of substitution, the more complicated these issues become. In addition, it is not hard to see that analogues of these difficulties will occur in the evaluation of the $\mathbf{H}_m$ matrix elements pertinent to the OS CCVB equations.

B. A CS formalism for OS CCVB

To circumvent these problems, we will transform the OS CCVB formalism into an *equivalent* CS one. For this, we introduce n_x "fictitious" orbitals with corresponding second quantization operators $\mathbf{b}^\dagger_{\kappa_\tau}$, with $\tau \in \{\alpha, \beta\}$. We group all the $\mathbf{b}_{\kappa_\tau}$ into a set $\mathcal{Q}_f$, and define $\mathcal{Q} = \mathcal{Q}_m \cup \mathcal{Q}_f$. We define $\mathbf{H}$ to be the second-quantization Hamiltonian that combines the main-system and fictitious orbitals, i.e. $\mathbf{H} = \hat{H}(\mathcal{Q})$.

We do not want electrons in the fictitious orbitals to have any meaningful physical effect on the main system, so we assume the fictitious orbitals are localized and we spatially separate them from each other and from the main system. In the limit of infinite separations, any core-Hamiltonian matrix element or any two-electron repulsion integral involving both fictitious and main-system orbitals, or any such matrix element involving more than one

fictitious orbital, will approach 0. Thus we can effectively assume any such element is 0. We may thus write

$$\mathbf{H} = \mathbf{H}_m + \mathbf{H}_f, \tag{22}$$

where $\mathbf{H}_f = \hat{H}(\mathcal{Q}_f)$, i.e. the Hamiltonian for the fictitious subsystem. It is not necessary to further elaborate on the fictitious orbitals. They are used for derivation purposes only, and indeed they will not appear in the final equations.

We now introduce a modified wave function:

$$|\boldsymbol{\psi}'\rangle = c_f \prod_{\kappa=n_\beta+1}^{n_\beta+n_x} \mathbf{b}^\dagger_{\kappa_\beta} |\boldsymbol{\psi}\rangle, \tag{23}$$

where c_f equals 1 or -1, which will be specified later. We can do this "addition" of fictitious orbitals to each of the configurations used to define $|\boldsymbol{\psi}\rangle$, such as $|\boldsymbol{\psi}_0\rangle$ and $|\boldsymbol{\psi}_{(ka)}\rangle$, and will likewise denote the resulting configurations by adding a prime. That is, for an arbitrary configuration $|\boldsymbol{\psi}_x\rangle$, we define

$$|\boldsymbol{\psi}'_x\rangle = c_f \prod_{\kappa=n_\beta+1}^{n_\beta+n_x} \mathbf{b}^\dagger_{\kappa_\beta} |\boldsymbol{\psi}_x\rangle. \tag{24}$$

Clearly

$$\langle \boldsymbol{\psi}'_x | \boldsymbol{\psi}' \rangle = \langle \boldsymbol{\psi}_x | \boldsymbol{\psi} \rangle. \tag{25}$$

Due to the spatial isolations of the fictitious electrons, we may write

$$\mathbf{H}_f |\boldsymbol{\psi}'\rangle = \boldsymbol{\epsilon}_f |\boldsymbol{\psi}'\rangle, \tag{26}$$

where $\boldsymbol{\epsilon}_f = \langle \boldsymbol{\psi}'_0 | \mathbf{H}_f | \boldsymbol{\psi}' \rangle$, i.e. the energy of the fictitious electrons. Using this and $\langle \boldsymbol{\psi}'_{(ka)} | \mathbf{H}_m | \boldsymbol{\psi}' \rangle = \langle \boldsymbol{\psi}_{(ka)} | \mathbf{H}_m | \boldsymbol{\psi} \rangle$, we obtain

$$\langle \boldsymbol{\psi}'_{(ka)} | \mathbf{H} | \boldsymbol{\psi}' \rangle - t_{ka} \boldsymbol{\epsilon}' = \xi_{ka}(\mathbf{t}), \tag{27}$$

where

$$\boldsymbol{\epsilon}' = \langle \boldsymbol{\psi}'_0 | \mathbf{H} | \boldsymbol{\psi}' \rangle = \boldsymbol{\epsilon} + \boldsymbol{\epsilon}_f. \tag{28}$$

Therefore the amplitude and energy equations of the modified wavefunction are equivalent to those of OS CCVB.

We now recall that the CCVB wave function, being of the valence-bond form, is an antisymmetrized product of spatial orbitals and a spin vector. Every (unprimed) OS CCVB configuration is also of this form. Therefore this is also true of the primed configurations

and $|\boldsymbol{\psi}'\rangle$. Because permutations of creation operators incur only a sign change at most, we can pair each fictitious orbital with an OS orbital of the main system. If the permutation causes a sign change, we set $c_f = -1$, otherwise it equals 1. This allows us to write

$$|\boldsymbol{\psi}'_0\rangle = \left(\prod_{k=1}^{n_\beta} \mathbf{g}^\dagger_{\mathbf{s},k}\right)\left(\prod_{\kappa=n_\beta+1}^{n_\beta+n_x} \mathbf{a}^\dagger_{\kappa_\alpha}\mathbf{b}^\dagger_{\kappa_\beta}\right)|0\rangle, \tag{29}$$

with analogous results for the other primed configurations and for $|\boldsymbol{\psi}'\rangle$. In other words, any primed configuration is alternatively obtained by taking its corresponding unprimed configuration, and every time an OS creation operator appears, we insert the corresponding β-spin fictitious creation operator on the right.

We thus have a set of n_α strongly orthogonal orbital pairs: the unmodified n_β pairs in the CS part of the wavefunction along with n_x pairs each consisting of one "real" OS orbital and one fictitious orbital. So, $|\boldsymbol{\psi}'\rangle$ is a product of strongly orthogonal orbital pairs and a spin vector. The spin vector here is not a total-spin eigenvector, but this property is needed to make a connection between OS and CS CCVB. We therefore consider

$$|\Psi\rangle \propto \mathbf{P}_{s=0}|\boldsymbol{\psi}'\rangle, \tag{30}$$

where $\mathbf{P}_{s=0}$ is the singlet orthogonal projection operator and normalization has been deferred for the time being. This projection does not change the spatial part of the wave function, so we now have a product of n_α strongly orthogonal orbital pairs and a singlet spin vector. Any such wavefunction is in the subspace spanned by the corresponding CS CCVB configurations, i.e. the ones built from these orbital pairs. By examining the expansion of $|\Psi\rangle$ in terms of these configurations, we will show that $|\Psi\rangle$ is of the coupled-cluster form.

In accord with our previous papers on CS CCVB, we will denote the present CS CCVB configurations by subscripted Ψ's. They are built up in the same basic way as used above for substitutions within the CS part of $|\boldsymbol{\psi}_0\rangle$, except that now the substitution processes include the OS pairs, i.e. the ones containing a fictitious electron. We therefore extend the applicability of eqs. (3) and (4) to the OS pairs by defining

$$\mathbf{a}^\dagger_{\lambda_\tau} = \mathbf{b}^\dagger_{\lambda_\tau}, \tag{31}$$

where τ is α or β, and fixing

$$\theta_\lambda = \frac{\pi}{2}, \tag{32}$$

i.e. the OS pairs are fully polarized.

The first term in the expansion concerns $|\Psi_0\rangle$. We are inclined to think of this configuration as the reference, and indeed it will soon become clear that this choice is justified, so

$$|\Psi\rangle = \frac{\mathbf{P}_{s=0}|\boldsymbol{\psi}'\rangle}{\langle\Psi_0|\boldsymbol{\psi}'\rangle}. \tag{33}$$

Note that in the denominator, $\mathbf{P}_{s=0}$ has been "absorbed" into $\langle\Psi_0|$ on the left, which is a property we will be using repeatedly.

Since we are interested in the details of $|\Psi\rangle$'s configuration expansion, our task is to look at the overlaps of the Ψ configurations with $|\Psi\rangle$. According to eq. (33), we need to evaluate the overlaps of the Ψ configurations with $|\boldsymbol{\psi}'\rangle$.

$|\boldsymbol{\psi}'\rangle$ is a linear combination of many configurations, but for each one the fictitious component of each OS pair is always β spin. Only the same kind of terms within any Ψ configuration will contribute to the pertinent overlap element. Take, for example, $\langle\Psi_0|\boldsymbol{\psi}'\rangle$. Looking at an OS pair, with index λ, $|\Psi_0\rangle$ has

$$\mathbf{g}^\dagger_{\mathbf{s},\lambda} = \frac{1}{\sqrt{2}}\left(-\mathbf{a}^\dagger_{\lambda_\alpha}\mathbf{b}^\dagger_{\lambda_\beta} - \mathbf{b}^\dagger_{\lambda_\alpha}\mathbf{a}^\dagger_{\lambda_\beta}\right) \tag{34}$$

there. Only the first product of creation operators in eq. (34) can contribute to $\langle\Psi_0|\boldsymbol{\psi}'\rangle$. If, in each OS pair in $|\Psi_0\rangle$, we were to remove the second product of creation operators, we would essentially be left with $|\boldsymbol{\psi}'_0\rangle$. Therefore

$$\langle\Psi_0|\boldsymbol{\psi}'\rangle = \left(\frac{-1}{\sqrt{2}}\right)^{n_x}\langle\boldsymbol{\psi}'_0|\boldsymbol{\psi}'\rangle = \left(\frac{-1}{\sqrt{2}}\right)^{n_x}. \tag{35}$$

We thus have an outline for working out the desired overlaps: for any Ψ configuration, we consider the removal of all components containing a fictitious α-spin orbital, and this results in a scalar multiple of a corresponding $\boldsymbol{\psi}'$ configuration whose overlap with $|\boldsymbol{\psi}'\rangle$ is already known. In general, we will denote the removal of fictitious α-spin terms with a $\xrightarrow{-\alpha'}$, as in

$$\mathbf{g}^\dagger_{\mathbf{s},\lambda} \xrightarrow{-\alpha'} \frac{-1}{\sqrt{2}}\mathbf{a}^\dagger_{\lambda_\alpha}\mathbf{b}^\dagger_{\lambda_\beta} \tag{36}$$

and

$$|\Psi_0\rangle \xrightarrow{-\alpha'} \left(\frac{-1}{\sqrt{2}}\right)^{n_x}|\boldsymbol{\psi}'_0\rangle. \tag{37}$$

Any Ψ configuration is a product of some number of $\mathbf{g}^\dagger_{\mathbf{s}}$, $\mathbf{d}^\dagger_{\mathbf{s_2}}$, and $\mathbf{e}^\dagger_{\mathbf{s_5}}$ operators acting on the vacuum state. Therefore removal of the fictitious α-spin terms from a configuration is

the same as removing them individually from each operator in the product that involves OS pairs. For 2-pair substitutions involving one CS and one OS pair, we have

$$\mathbf{d}^\dagger_{\mathbf{s_2},k\lambda} \xrightarrow{-\alpha'} \frac{-1}{\sqrt{2}}\mathbf{d}^\dagger_{\mathbf{d_2},k\lambda}\mathbf{b}^\dagger_{\lambda_\beta}, \tag{38}$$

and for 2-pair substitutions involving two OS pairs we have

$$\mathbf{d}^\dagger_{\mathbf{s_2},\kappa\lambda} \xrightarrow{-\alpha'} \frac{1}{2\sqrt{3}}\mathbf{a}^\dagger_{\kappa_\alpha}\mathbf{b}^\dagger_{\kappa_\beta}\mathbf{a}^\dagger_{\lambda_\alpha}\mathbf{b}^\dagger_{\lambda_\beta}. \tag{39}$$

For 3-pair substitutions involving two CS pairs and one OS pair, we have

$$\mathbf{e}^\dagger_{\mathbf{s_5},kl\mu} \xrightarrow{-\alpha'} \frac{-1}{\sqrt{2}}\mathbf{e}^\dagger_{\mathbf{d_5},kl\mu}\mathbf{b}^\dagger_{\mu_\beta}, \tag{40}$$

for 3-pair substitutions involving one CS pair and two OS pairs we have

$$\begin{aligned}\mathbf{e}^\dagger_{\mathbf{s_5},k\lambda\mu} \xrightarrow{-\alpha'} \frac{1}{\sqrt{6}}\Big(&-\mathbf{g}^\dagger_{\mathbf{t_2},k}(\frac{-1}{\sqrt{2}}\mathbf{a}^\dagger_{\lambda_\alpha}\mathbf{b}^\dagger_{\lambda_\beta})\mathbf{a}^\dagger_{\mu_\beta}\mathbf{b}^\dagger_{\mu_\beta}\\ &+\mathbf{g}^\dagger_{\mathbf{t_2},k}\mathbf{a}^\dagger_{\lambda_\beta}\mathbf{b}^\dagger_{\lambda_\beta}(\frac{-1}{\sqrt{2}}\mathbf{a}^\dagger_{\mu_\alpha}\mathbf{b}^\dagger_{\mu_\beta})\Big)\\ =\frac{-1}{\sqrt{2}}\frac{1}{2}\Big(&\mathbf{d}^\dagger_{\mathbf{d_2},k\lambda}\mathbf{b}^\dagger_{\lambda_\beta}\mathbf{a}^\dagger_{\mu_\alpha}\mathbf{b}^\dagger_{\mu_\beta}\\ &-\mathbf{d}^\dagger_{\mathbf{d_2},k\mu}\mathbf{b}^\dagger_{\mu_\beta}\mathbf{a}^\dagger_{\lambda_\alpha}\mathbf{b}^\dagger_{\lambda_\beta}\Big),\end{aligned} \tag{41}$$

and for 3-pair substitutions involving 3 OS pairs we have

$$\mathbf{e}^\dagger_{\mathbf{s_5},\kappa\lambda\mu} \xrightarrow{-\alpha'} 0. \tag{42}$$

The preceding equations show that

$$|\Psi_{(kl)}\rangle \xrightarrow{-\alpha'} \left(\frac{-1}{\sqrt{2}}\right)^{n_x}|\boldsymbol{\psi}'_{(kl)}\rangle, \tag{43}$$

$$|\Psi_{(k\lambda)}\rangle \xrightarrow{-\alpha'} \left(\frac{-1}{\sqrt{2}}\right)^{n_x}|\boldsymbol{\psi}'_{(k\lambda)}\rangle, \tag{44}$$

$$|\Psi_{(\kappa\lambda)}\rangle \xrightarrow{-\alpha'} \frac{1}{\sqrt{3}}\left(\frac{-1}{\sqrt{2}}\right)^{n_x}|\boldsymbol{\psi}'_0\rangle, \tag{45}$$

$$|\Psi_{(klm)}\rangle \xrightarrow{-\alpha'} \left(\frac{-1}{\sqrt{2}}\right)^{n_x}|\boldsymbol{\psi}'_{(klm)}\rangle, \tag{46}$$

$$|\Psi_{(kl\mu)}\rangle \xrightarrow{-\alpha'} \left(\frac{-1}{\sqrt{2}}\right)^{n_x}|\boldsymbol{\psi}'_{(kl\mu)}\rangle, \tag{47}$$

$$|\Psi_{(k\lambda\mu)}\rangle \xrightarrow{-\alpha'} \left(\frac{-1}{\sqrt{2}}\right)^{n_x+1}\Big(|\boldsymbol{\psi}'_{(k\lambda)}\rangle - |\boldsymbol{\psi}'_{(k\mu)}\rangle\Big), \tag{48}$$

and

$$|\Psi_{(\kappa\lambda\mu)}\rangle \xrightarrow{-\alpha'} 0. \tag{49}$$

Using the preceding equations along with eqns. (33) and (35), we get

$$\langle\Psi_{(kl)}|\Psi\rangle = t_{kl}, \tag{50}$$

$$\langle\Psi_{(k\lambda)}|\Psi\rangle = t_{k\lambda}, \tag{51}$$

$$\langle\Psi_{(\kappa\lambda)}|\Psi\rangle = \frac{1}{\sqrt{3}}, \tag{52}$$

$$\langle\Psi_{(klm)}|\Psi\rangle = \langle\Psi_{(kl\mu)}|\Psi\rangle = \langle\Psi_{(\kappa\lambda\mu)}|\Psi\rangle = 0, \tag{53}$$

and

$$\langle\Psi_{(k\lambda\mu)}|\Psi\rangle = \frac{-1}{\sqrt{2}}(t_{k\lambda} - t_{k\mu}). \tag{54}$$

We turn now to 4-pair substitutions, $|\Psi_{(ab)(cd)}\rangle$. The evaluation of the inner product with $|\Psi\rangle$ is conceptually not much different from the above steps. We have a product of two $\mathbf{d}^\dagger_{\mathbf{s_2}}$'s and potentially several $\mathbf{g}^\dagger_{\mathbf{s}}$'s acting on the vacuum state. We select those operators in this product that involve OS pairs and remove the fictitious α-spin terms by using eqns. (36), (38), and (39) as needed. Regardless of the number of OS pairs involved in the substituted part of the configuration, we obtain

$$\langle\Psi_{(ab)(cd)}|\Psi\rangle = t_{ab}t_{cd}, \tag{55}$$

where we have defined

$$t_{\kappa\lambda} = \frac{1}{\sqrt{3}}. \tag{56}$$

Therefore the conversion of OS CCVB into a CS form preserves the coupled-cluster nature of the wavefunction. For the present purposes, it is not necessary to consider higher order substitutions.

Much of our intended OS-to-CS connection has been made, but we still need to draw a parallel to the OS CCVB equations. For this, consider

$$\Omega_{ab}(\mathbf{t}) = \langle\Psi_{(ab)}|\mathbf{H}|\Psi\rangle - t_{ab}E, \tag{57}$$

where

$$E = \langle\Psi_0|\mathbf{H}|\Psi\rangle. \tag{58}$$

These have the same form as the amplitude and energy equations of ordinary CS CCVB. To elucidate the relevance of these equations to the task at hand, we must examine inner products of CS CCVB configurations with $\mathbf{H}|\Psi\rangle$. For a general Ψ configuration, $|\Psi_x\rangle$, we have

$$\langle\Psi_x|\mathbf{H}|\Psi\rangle = \frac{1}{\langle\Psi_0|\boldsymbol{\psi}'\rangle}\langle\Psi_x|\mathbf{H}|\boldsymbol{\psi}'\rangle, \tag{59}$$

where we have used the fact that $\mathbf{P}_{s=0}$ and $\mathbf{H}$ commute, and absorbed $\mathbf{P}_{s=0}$ into $\langle\Psi_x|$ as done above. So, the inner products of CS CCVB configurations with $\mathbf{H}|\Psi\rangle$ boil down to inner products of the configurations with $\mathbf{H}|\boldsymbol{\psi}'\rangle$.

Like $|\boldsymbol{\psi}'\rangle$, the fictitious parts of $\mathbf{H}_m|\boldsymbol{\psi}'\rangle$, and those of $\boldsymbol{\epsilon}_f|\boldsymbol{\psi}'\rangle$, are only β-spin. This is therefore also true of $\mathbf{H}|\boldsymbol{\psi}'\rangle$. So, just like we did repeatedly above, we can simplify the inner product of interest, $\langle\Psi_x|\mathbf{H}|\boldsymbol{\psi}'\rangle$, by removing the fictitious α-spin terms of the involved Ψ configuration, $\langle\Psi_x|$.

Substituting eqns. (37) and (43)-(45) into eq. (59), we obtain

$$E = \boldsymbol{\epsilon}', \tag{60}$$

$$\langle\Psi_{(kl)}|\mathbf{H}|\Psi\rangle = \langle\boldsymbol{\psi}'_{(kl)}|\mathbf{H}|\boldsymbol{\psi}'\rangle, \tag{61}$$

$$\langle\Psi_{(k\lambda)}|\mathbf{H}|\Psi\rangle = \langle\boldsymbol{\psi}'_{(k\lambda)}|\mathbf{H}|\boldsymbol{\psi}'\rangle, \tag{62}$$

and

$$\langle\Psi_{(\kappa\lambda)}|\mathbf{H}|\Psi\rangle = \frac{1}{\sqrt{3}}\langle\boldsymbol{\psi}'_0|\mathbf{H}|\boldsymbol{\psi}'\rangle = t_{\kappa\lambda}E. \tag{63}$$

Combining these results with eq. (27), we have

$$\Omega_{ka}(\mathbf{t}) = \xi_{ka}(\mathbf{t}), \tag{64}$$

and we also see that the equations $\Omega_{\kappa\lambda}(\mathbf{t}) = 0$ are automatically satisfied, whether or not the fully CS or mixed CS-OS equations are satisfied.

C. Implementing OS CCVB

Our approach to computing OS CCVB in a CS CCVB context thus boils down to solving the Ω equations, i.e. finding a set of amplitudes such that each $\Omega_{ab}(\mathbf{t}) = 0$. This meets the conditions of our original goal, because we can now use the simpler machinery, namely configurations, of CS CCVB to handle these equations and any other required elements,

such as the energy. For the first part of $\Omega_{ab}(\mathbf{t})$, i.e. $\langle\Psi_{(ab)}|\mathbf{H}|\Psi\rangle$, we observe that $\langle\Psi_{(ab)}|$ can interact through $\mathbf{H}$ with the reference and the configurations with 2-pair, 3-pair, and 4-pair substitutions, but not higher. From eq. (55), the structure of the 4-pair substituted part of $|\Psi\rangle$ is the same as that of regular CS CCVB. Therefore, except for the 3-pair terms, $\langle\Psi_{(ab)}|\mathbf{H}|\Psi\rangle$ is identical in form to its counterpart of regular CS CCVB.

For the second part of $\Omega_{ab}(\mathbf{t})$, i.e. $t_{ab}E$ or $t_{ab}\langle\Psi_0|\mathbf{H}|\Psi\rangle$, we observe that $\langle\Psi_0|$ can interact through $\mathbf{H}$ with the reference and the configurations with 2-pair substitutions, but not higher. Therefore this part is identical in form to its counterpart in regular CS CCVB. We see that $\Omega_{ab}(\mathbf{t})$ is equal to its regular CS CCVB counterpart, which will be denoted in this paper by $\mathrm{R}_{ab}(\mathbf{t})$, plus a term for the 3-pair substitutions. In eq. (28) of ref. 59, it is shown that

$$\mathrm{R}_{ab}(\mathbf{t}) = \mu_{ab}(1-t_{ab}^2) + t_{ab}\omega_{ab} + \sum_{c\notin\{a,b\}}\Big[t_{ac}(\kappa_{bc}-t_{ab}\mu_{ac}) + t_{bc}(\kappa_{ac}-t_{ab}\mu_{bc})\Big], \tag{65}$$

where

$$\kappa_{bc} = \langle\Psi_{(ab)}|\mathbf{H}|\Psi_{(ac)}\rangle, \tag{66}$$

$$\mu_{ab} = \langle\Psi_0|\mathbf{H}|\Psi_{(ab)}\rangle, \tag{67}$$

and

$$\omega_{ab} = \langle\Psi_{(ab)}|\mathbf{H}|\Psi_{(ab)}\rangle - \langle\Psi_0|\mathbf{H}|\Psi_0\rangle. \tag{68}$$

The other main differences between the modified CS CCVB and regular CS CCVB are that we must fix the values of the fully OS amplitudes according to eq. (56) and that we need to properly deal with the fictitious elements.

In the general case, the only 3-pair substituted configurations that $\langle\Psi_{(ab)}|$ can interact with through $\mathbf{H}$ are the ones that share both indices a and b. For this, we define

$$\kappa_{ab;c} = \langle\Psi_{(ab)}|\mathbf{H}|\Psi_{(abc)}\rangle. \tag{69}$$

The only 3-pair substitutions with non-zero amplitudes in the current context are the ones with two OS indices, so the 3-pair substitutions do not enter the various $\Omega_{kl}(\mathbf{t})$, i.e. they do not (directly) affect the fully CS amplitude equations. Indeed, these equations are identical in form to those of regular CS CCVB:

$$\Omega_{kl}(\mathbf{t}) = \mathrm{R}_{kl}(\mathbf{t}). \tag{70}$$

The 3-pair substitutions show up in the partially OS equations:

$$\Omega_{k\lambda}(\mathbf{t}) = \mathrm{R}_{k\lambda}(\mathbf{t}) - \frac{1}{\sqrt{2}} \sum_{\mu \neq \lambda} \Big[\kappa_{k\lambda;\mu}(t_{k\lambda} - t_{k\mu}) \Big]. \tag{71}$$

Simplified expressions for the μ, κ, and ω elements found in $\mathrm{R}_{ab}(\mathbf{t})$, and a description of their efficient computation, have been presented in ref. 60. These matrix elements boil down to three basic quantities: (1) single-pair one-electron contributions:

$$\eta_{a;\,\mathbf{wx}} = \sum_{p,r \in S_a} h_{pr} P_{a;\,\mathbf{wx};\,pr}, \tag{72}$$

where $\mathbf{w}, \mathbf{x} \in \{\mathbf{s}, \mathbf{t_1}, \mathbf{t_2}, \mathbf{t_3}\}$, the h_{pr} are core-Hamiltonian matrix elements, $S_a = \{a_\alpha, \hat{a}_\alpha, a_\beta, \hat{a}_\beta\}$, and

$$P_{a;\,\mathbf{wx};\,pr} = \langle 0 | \mathbf{g}_{\mathbf{w},a} \mathbf{a}_p^\dagger \mathbf{a}_r \mathbf{g}_{\mathbf{x},a}^\dagger | 0 \rangle; \tag{73}$$

(2) intrapair electron repulsion:

$$\rho_{a;\,\mathbf{w};\,\mathbf{x}} = \sum_{p,q} \sum_{r,s} \langle pq||rs\rangle f_{a;\,\mathbf{w};\,pq} f_{a;\,\mathbf{x};\,rs}, \tag{74}$$

where the $\langle pq||rs\rangle$ are ordinary antisymmetrized two-electron integrals and the $f_{a;\,\mathbf{w}}$ contain the expansion coefficients for the corresponding geminals; and (3) interpair electron repulsion:

$$\sigma_{ab;\,\mathbf{wx};\,\mathbf{yz}} = \sum_{p,r \in S_a} \sum_{q,s \in S_b} \langle pq||rs\rangle P_{a;\,\mathbf{wx};\,pr} P_{b;\,\mathbf{yz};\,qs}. \tag{75}$$

Eq. (73) defines various density matrices associated with a given electron pair. The elements of these density matrices are given explicitly in ref. 60, as are the various $f_{a;\,\mathbf{w}}$ elements, which may also be directly inferred above in eqs. (3) and (4).

Employing the same basic approach used in ref. 60 to simplify the expression for the μ_{kl} elements (c.f. eqs. (19), (20), and (25) there), it may be shown that

$$\kappa_{ab;c} = \langle 0 | \mathbf{d}_{\mathbf{s_2},ab} \mathbf{g}_{\mathbf{s},c}\, \mathbf{H}\, \mathbf{e}_{\mathbf{s_5},abc}^\dagger | 0 \rangle = \sqrt{6}\, \langle 0 | \mathbf{d}_{\mathbf{s_2},ab} \mathbf{g}_{\mathbf{s},c}\, \mathbf{H}\, \mathbf{g}_{\mathbf{t_1},a}^\dagger \mathbf{g}_{\mathbf{t_2},b}^\dagger \mathbf{g}_{\mathbf{t_3},c}^\dagger | 0 \rangle, \tag{76}$$

where we have used the fact that the singlet projection of $\sqrt{6}\, \mathbf{g}_{\mathbf{t_1},a}^\dagger \mathbf{g}_{\mathbf{t_2},b}^\dagger \mathbf{g}_{\mathbf{t_3},c}^\dagger | 0 \rangle$ is $\mathbf{e}_{\mathbf{s_5},abc}^\dagger | 0 \rangle$. We then obtain an expression for $\kappa_{ab;c}$ that is amenable to efficient computation:

$$\kappa_{ab;c} = \sqrt{2}(\sigma_{bc;\,\mathbf{t_1 t_2};\,\mathbf{s t_3}} - \sigma_{ac;\,\mathbf{t_3 t_1};\,\mathbf{s t_3}}). \tag{77}$$

At this point, we have expressions suitable for computation for all the matrix elements found in the CCVB equations. Technically, some of these matrix elements involve the

fictitious orbitals. However, due to eq. (64), any such component gets cancelled out in the CCVB equations. It is therefore legitimate to remove every fictitious term from the outset. Every pertinent matrix element reduces to an expression involving η, ρ, and σ terms, and in turn these boil down to basic one and two electron integrals multiplied by either the geminal expansion coefficients or the pair-based density matrices. Thus, we can remove all fictitious terms by simply deleting (or zeroing) every element with a hatted index of every $P_{\lambda;\mathbf{wx}}$ matrix and every $f_{\lambda;\mathbf{w}}$ vector, and then directly using these modified density matrices and geminal expansion coefficient vectors in the expressions for the matrix elements in the same way as is done for the CS pairs. The energy computed in this way is equal to $\boldsymbol{\epsilon}$.

We have thus established a framework for obtaining the cluster amplitudes and thereby the CCVB energy, and we can now discuss how this gets implemented computationally. The principle objective of a CCVB calculation is to find orbitals that minimize the energy. In line with the above development, the computational implementation of the present modified CS CCVB closely mirrors that of regular CS CCVB. A detailed description of the latter is found in ref. 60, so we will focus here on giving a broad overview, providing notes specific to the OS context as needed.

For the orbital optimization, we introduce a Lagrangian

$$\Lambda = E + \sum_{k<a} \lambda_{ka} \Omega_{ka}(\mathbf{t}), \tag{78}$$

with Lagrange multipliers λ_{ka}, which will also be referred to as $\boldsymbol{\lambda}$ amplitudes. At every iteration of the optimization, we must compute the gradient of Λ with respect to orbital rotations and the θ_k, which we will refer to collectively as the orbital variables. Of course, this requires that we first compute the $\mathbf{t}$ and $\boldsymbol{\lambda}$ amplitudes. We use a nonlinear Gauss-Seidel iterative procedure to solve the $\mathbf{t}$ equations, i.e. $\Omega_{ka}(\mathbf{t}) = 0$, and we use linear Gauss-Seidel iterations to solve the $\boldsymbol{\lambda}$ equations, which are obtained by differentiating Λ with respect to the $\mathbf{t}$ amplitudes.

Once the amplitudes have been computed, we compute the θ_k gradient of Λ. We recall that the current Λ differs from that of regular CS CCVB only in the terms related to 3-pair substitutions. However, $\kappa_{k\lambda;\mu}$ does not depend on θ_k, so the 3-pair substitution terms have no dependence on any of the θ_k. Therefore, we simply reuse the code for regular CS CCVB here. See section II.B.6 of ref. 60.

To compute the orbital-rotation gradient of Λ, we express Λ in terms of overall one and

two electron density matrices Γ (c.f. eq. (50) of ref. 60):

$$\Lambda = \sum_{pq} \Gamma_{pq} g_{pq} + \sum_{pqrs} \Gamma_{pqrs} \mathbb{M}_{pqrs}, \tag{79}$$

where the indices here correspond to spatial orbitals and g_{pq} and $\mathbb{M}_{pqrs}$ are core-Hamiltonian elements and two electron repulsion intregrals, respectively, the latter not antisymmetrized. These density matrices are computed on the fly, based on expressing Λ in terms of the various η, ρ, and σ terms. For the regular CS CCVB Λ, this expression is shown in eq. (51) of ref. 60. For the current context, we can use this expression with a modification to account for the 3-pair substitution terms, which is easily obtained by combining eqs. (71) and (77). Then, every time a η, ρ, or σ term occurs in this expression, we call a function that cumulatively adds to the Γ elements pertinent to that term. More details on this procedure are given in section II.B.4 of ref. 60.

The CCVB orbital optimization is guided by the Geometric Direct Minimization (GDM) method,[68] which utilizes the first derivatives of an objective function, in this case Λ, to take a "step", i.e. an energy reducing change in the values of the orbital variables. In GDM, convergence is enhanced by the inclusion of diagonal second derivatives. As with the first derivatives with respect to the θ_k, we can reuse the regular CS CCVB code for the corresponding second derivatives.

Each diagonal second derivative of Λ with respect to the orbital rotation parameters may be separated into two terms, one of which directly involves the Λ orbital rotation gradient, while the other is approximated by its counterpart in the corresponding second derivative of the reference energy, $\langle \Psi_0 | \mathbf{H} | \Psi_0 \rangle$. See section II.B.5 of ref. 60. We again reuse the regular CS CCVB code here.

This concludes our discussion of the orbital optimization algorithm. We have implemented it in the Q-Chem electronic structure program,[69] and we will now illustrate its usage with some molecular examples.

III. CALCULATIONS

In this section, all CCVB, Hartree Fock, and DFT calculations used the Q-Chem program,[69] and all CASSCF calculations used the GAMESS program.[70] Except in Sec. III C below, basis-set parameters were obtained from the Basis Set Exchange.[71,72] Except

where stated otherwise, all calculations used Cartesian d and f orbitals.

A. P_2

The first example is the P_2 molecule. We will use the cc-pVDZ basis.[73] P_2 provides a good test for MR methods for the same reason that its ubiquitous cousin N_2 does: the dissociation of its singlet ground state entails a broken triple bond. We will apply CCVB to this state and also to P_2's lowest triplet and quintet states, which, along with the lowest septet, also dissociate into two quartet-spin P atoms. The separated atoms each have three unpaired electrons, so we need at least a (6,6) active space to obtain qualitative accuracy, and this is what will be used here. We will use (6,6) CASSCF calculations to benchmark the CCVB results. For the septet state in this active space, CCVB and CASSCF are the same as restricted OS HF (ROHF), and the potential energy surface (PES) is repulsive. For these reasons, we will not present data on this state.

To obtain the CCVB results, we first produced the singlet PES. For this, we picked one geometry and used the RHF-based initial guess procedure described previously.[60] Then, for every other geometry, we read in the parameters from a geometrically adjacent, previously converged calculation. We then obtained a CCVB PES for the triplet as follows. The basic form of the CCVB active space in this case is two strongly orthogonal CS pairs and two singly occupied orbitals, the latter constituting an $s_z = 1$ triplet. We can obtain an initial guess conforming to these specifications by simply converting one of the CS pairs from the singlet calculation into an $s_z = 1$ triplet.

Given that the CS pairs have singlet form in the reference wave function, and that for two electrons, singlet and triplet states are most similar when the singlet is a perfect biradical, the required conversion of a CS pair to an $s_z = 1$ triplet is most natural for the most polarized CS pair. Therefore, at one geometry, we took the most polarized pair from the CCVB singlet calculation and reassigned two orthogonal orbitals spanning that pair (it does not matter which ones) to be singly occupied. As with the singlet, the remainder of the triplet PES was obtained sequentially by reading in parameters from adjacent geometries. The CCVB quintet was obtained using the same basic idea. In this case, for the starting geometry, the two most polarized pairs of the CCVB singlet get converted to four singly occupied orbitals.

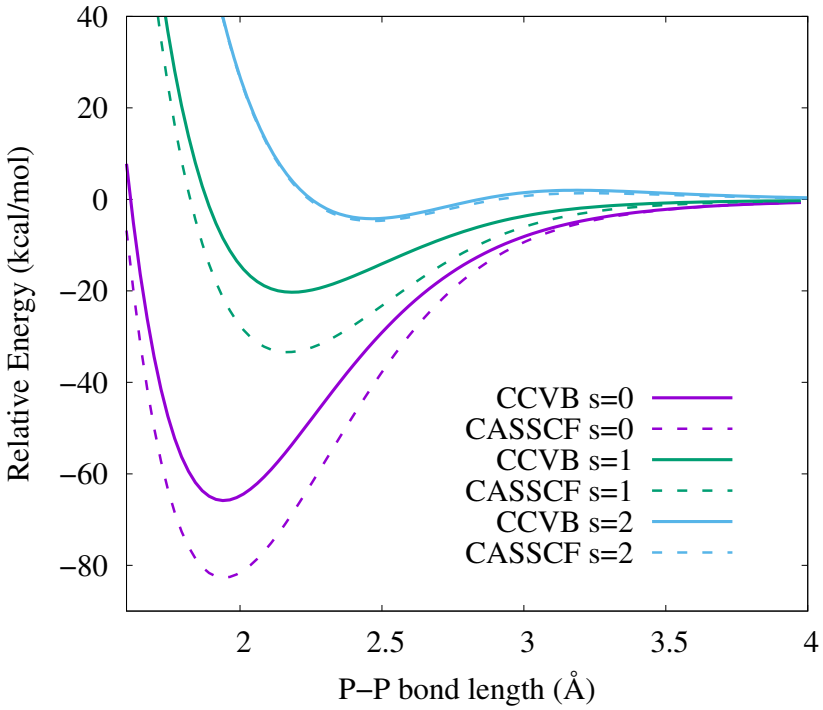

FIG. 1: P_2 CCVB and CASSCF PESs. Energies are relative to two times the $s = 3/2$ ROHF energy for P, and use 6 active electrons in 6 orbitals.

For the CCVB singlet, the three pairs correspond to the σ and π bonds. The π-bond pairs are equally polarized and are more polarized than the σ-bond pair. So, for the CCVB triplet, two of the π electrons make up a CS pair and the other two are singly occupied. This may entail some spatial symmetry breaking. This is not an issue for the quintet, where all four π electrons are singly occupied. Finally, every CASSCF calculation (at every geometry) used as an initial guess the converged CCVB orbitals for the corresponding spin state.

The CCVB and CASSCF results are presented in Fig. 1. Our first observation is that all three CCVB curves dissociate to the correct atomic limit. This is achieved through interpair correlation. For the singlet, in the dissociation limit, all interpair amplitudes approach $\sqrt{3}^{-1}$ in absolute value. The same basic thing occurs for the triplet and quintet. For those states, all interpair CS/CS *and* CS/OS amplitudes reach the same limit (in absolute value). In other words, the unpaired electrons are strongly coupled to the paired ones as the bond is broken.

To emphasize the fact that achieving the correct dissociation limit for $s = 1, 2$ is non-

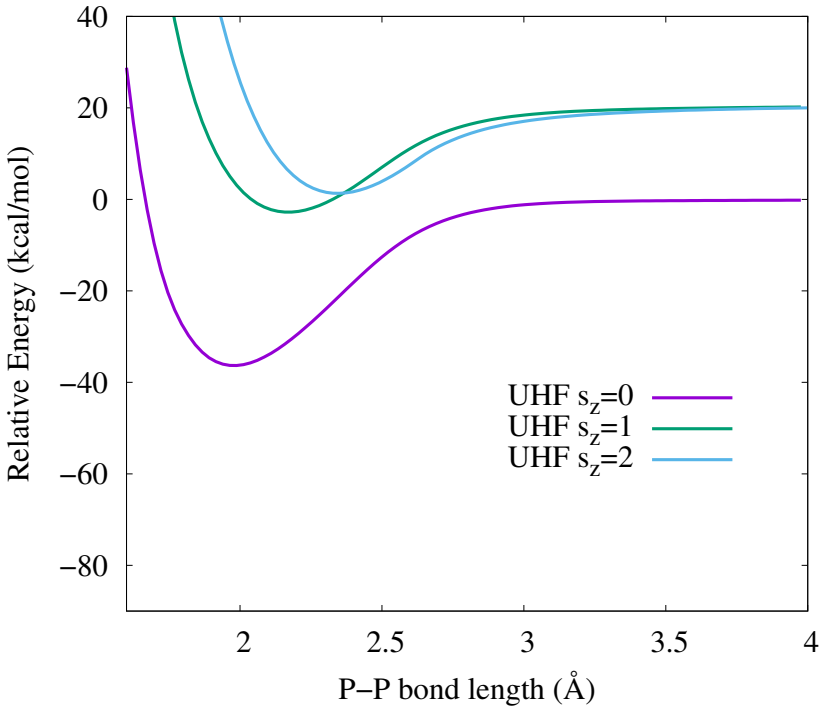

FIG. 2: P_2 UHF PESs. Energies are relative to two times the $s_z = 3/2$ UHF energy for P.

trivial, we have included UHF data in Fig. 2. Following standard UHF procedure, we performed UHF calculations with 0, 2, and 4 excess α electrons, which are to approximate the singlet, triplet, and quintet, respectively. Only the $s_z = 0$ curve dissociates to the correct limit. Each of the other two curves dissociates to a limit where one atom has three spin-aligned p electrons and likewise for the second atom but with one of its p-electron spins flipped. The second atom has $\|s_z\| = 0.5$ and is a mixture of doublet and quartet states; hence the higher energy. In broader terms, UHF (and UDFT) does not provide a physically correct description of the dissociation of most of the spin states of a given system. We will encounter this again in examples below.

Returning to Fig. 1, we see that each CCVB curve stays above its CASSCF counterpart, which is in line with our long experience: we have yet to observe CCVB break variational bounds, although the method is not formally constrained in this way. We also see that for the singlet and triplet, there is a noticable gap between CCVB and CASSCF in the equilibrium regions. This is the expected result because, in terms of dimensionality, CCVB represents only a small part of the complete active space for these two states. Using VB language, the

ionic configurations not included in CCVB play a significant quantitative role. However, this is evidently not the case for the quintet. Ignoring spatial symmetry, the dimension of the (6,6) quintet active space is only 35.

B. Mn_2^+

We turn now to a more complicated example, the dissociation of the Manganese dimer cation, Mn_2^+, in various spin states. We will use the Wachters+f basis set.[74–76] This is a compact, augmented triplet zeta plus polarization basis, and it meets the criteria recommended for Mn in ref. 77.

The ground-state electron configurations of Mn and Mn^+ are $4s^2 3d^5$ (sextet spin) and $4s^1 3d^5$ (septet spin), respectively, and these states are (spatially) nondegenerate. Thus the lowest-energy $s = \frac{1}{2}, \frac{3}{2}, \frac{5}{2}, \frac{7}{2}, \frac{9}{2}, \frac{11}{2}$ states of the molecule will dissociate to ground-state atoms, and these states will be the focus of this subsection. Experimental studies[78–80] as well as most computational work,[81,82] has concluded that the ground state is maximally ferromagnetic. We note that each of these spin values will actually present two states, one gerade and one ungerade, that dissociate in this way, because of the equivalence of Mn^+-Mn and Mn-Mn^+.

The states of interest here require (at least) an (11,11) active space, whereas a full valence active space would be (13,12). Using (11,11) means placing two valence electrons in an inactive (valence) orbital. In principle, this is reasonable because, using simplified terms, we would expect the dominant configuration to have $\sigma_g(4s)^2\sigma_u(4s)^1$, owing to the fact that the atomic dissociation products have three electrons occupying the two $4s$ orbitals. For CCVB, the alternative to (11,11) would be to use a (13,13) active space, which entails using one orbital lying outside the valence level. With the preceding points in mind, we will use the (11,11) active space here.

To verify our usage of (11,11) in practice, we did both (13,12) and (11,11) CASSCF calculations on the doublet at a bond length of 3 Å (a geometry choice which will become clear when we show full PESs later). The (13,12) and (11,11) CASSCF energies differ by only 0.06 kcal/mol, and in (13,12) the highest occupation number has a value of 1.9995, with the corresponding natural orbital having σ symmetry with predominantly $4s$ contributions. Therefore, (11,11) should be adequate for this system. It should be noted that CASSCF (and CCVB) break spatial symmetry for this molecule. In both the (13,12) and (11,11) CASSCF

calculations, the just mentioned orbital breaks inversion symmetry, gradually localizing to one atom as the bond length increases. A similar thing occurs for the other (essentially singly occupied) 4*s*-dominant orbital. A driving force for this symmetry breaking is that, in an active space calculation, the optimal orbitals for Mn differ quantitatively from those of Mn^+. To be consistent with this in the dissociation limit, the CASSCF and CCVB orbitals must localize and thereby break symmetry. Of course, given symmetric orbitals, valence space or full space FCI calculations will respect $D_{\infty h}$ symmetry.

We obtained CCVB PESs for the various spin states as follows. At one geometry, we computed the lowest-energy UHF solution for $s_z = 0.5$. We used this UHF solution to get an initial guess for the CCVB doublet, following the procedure discussed earlier.[60] As used for P_2, we then computed the rest of the CCVB doublet PES by sequentially reading in guesses from adjacent geometries. As discussed above for P_2, we selected one geometry and converted the most polarized pair from the doublet calculation into an $s_z = 1$ triplet and used this as an initial guess for a quartet calculation at that geometry. The rest of the CCVB quartet PES was computed using the adjacent-geometry sequential approach. We iterated this basic idea to compute the remaining CCVB PESs: starting from the same doublet solution, we converted increasing numbers of CS pairs to triplets to get guesses for the other spin states, finishing each PES sequentially as above. We then used these CCVB results to compute all the CASSCF PESs: every CASSCF calculation used its counterpart CCVB orbitals as an initial guess, as was done for P_2.

In order of increasing polarization, the CCVB doublet's five CS pairs have Σ, Π, and Δ symmetry, and this determines the division between CS and OS for the higher spin states. For example, two of the three unpaired electrons of the quartet have Δ symmetry while the remaining one is Σ. This leaves one Δ CS pair, and the situation is thus like the P_2 triplet, where two of the four Π electrons were in a CS pair while the remaining two were OS.

The results of our CCVB calculations are given in Fig. 3. We did not include CASSCF results in this figure because they are very close to the CCVB results and it is difficult to visually distinguish the two methods on this scale. Instead, we have plotted the energy difference between CCVB and CASSCF for each spin state in Fig. 4. As was the case for the P_2 quintet, the ionic configurations not included in CCVB do not make much of a contribution to the CASSCF energies for any of the Mn_2^+ spin states. This appears to be due, in large part, to a long bond length and relatively high valence level, and it is consistent

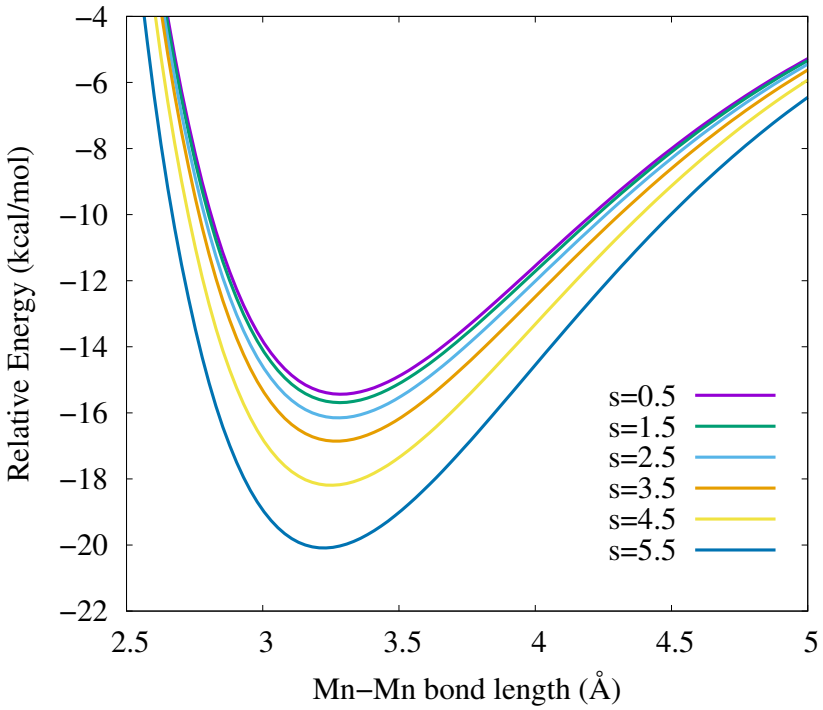

FIG. 3: Mn_2^+ CCVB PESs. Energies are relative to the sum of the $s = 5/2$ and $s = 3$ ROHF energies for Mn and Mn^+, respectively, and are evaluated using 11 electrons in 11 orbitals.

with previous CCVB calculations on the singlet ground state of Cr_2.[69]

A curious feature of Mn_2^+ is that the energy ordering of its spin states is opposite to that for P_2. The duodecet ($s = \frac{11}{2}$) is the ground state here, and this is why we have included it in Fig. 3, despite the fact that for this state, CCVB(11,11) and CASSCF(11,11) are equivalent and are the same as ROHF, similar to the case of the P_2 septet.

We next observe that CCVB is able to properly dissociate all the pertinent spin states. As with P_2, this entails full interpair (both CS/CS and CS/OS) correlation in the dissociation limit. For comparison, UHF can reach the correct energy at full separation for $s_z = \frac{1}{2}$ and $s_z = \frac{11}{2}$ calculations but cannot do so for $s_z = \frac{3}{2}, \frac{5}{2}, \frac{7}{2}, \frac{9}{2}$ calculations. Continuing to look at longer bond lengths (e.g. 5 Å), we see that the relative energies of the Mn_2^+ states are significantly below zero, and it is evident that electrostatic effects are significantly responsible for this observation. The difference between the binding energy obtained for $s = \frac{11}{2}$ (about 20 kcal/mol) and the values obtained experimentally[83] or by calculations

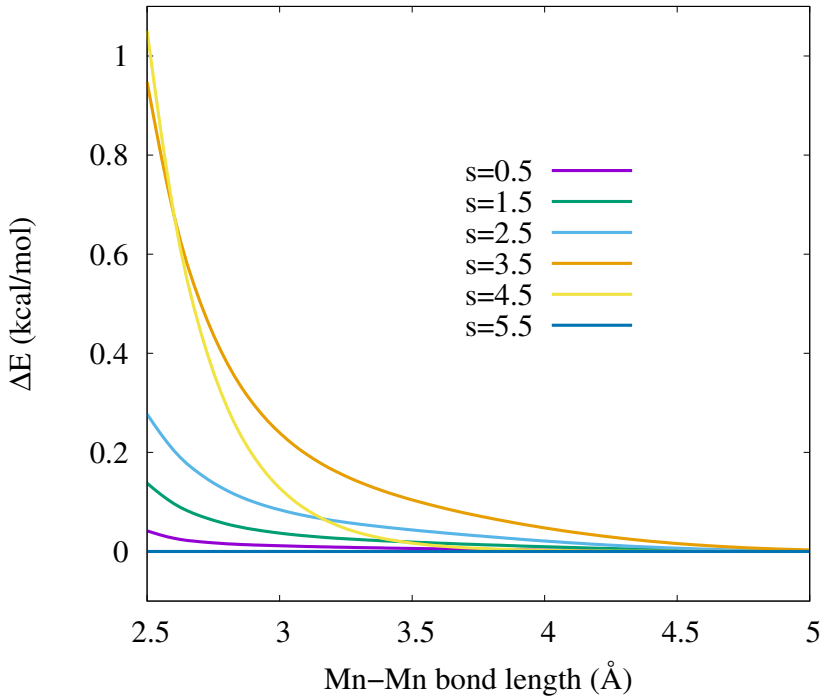

FIG. 4: Energy difference between (11,11) CCVB and (11,11) CASSCF for Mn_2^+ PESs.

that treat all correlation effects[81] (about 32 kcal/mol) reflect dispersion and other dynamic correlation contributions.

C. Model Polycarbenes

We focus next on polycarbenes, i.e. organic molecules with several carbene sites. In particular, we are interested in triplet carbene sites. These units, separated by appropriate organic linkers, may couple to form various overall spin states, most of which will be strongly correlated. A paradigm for this is found in the various quasi-one-dimensional chains of triplet carbenes separated by phenyl groups. The latter serve as "ferromagnetic coupling units" (fCUs),[65,84,85] causing the spins on adjacent carbenes to align in a maximal-spin ground state, at least up to oligomers of moderate size. These systems have received significant experimental and theoretical attention,[66,67,86–96] and they serve as a basis for the present work.

To enable calculations on large chains with many carbene sites, we chose to study simplified model systems in which the phenyl linkers have been replaced by CH_2 linkers. More

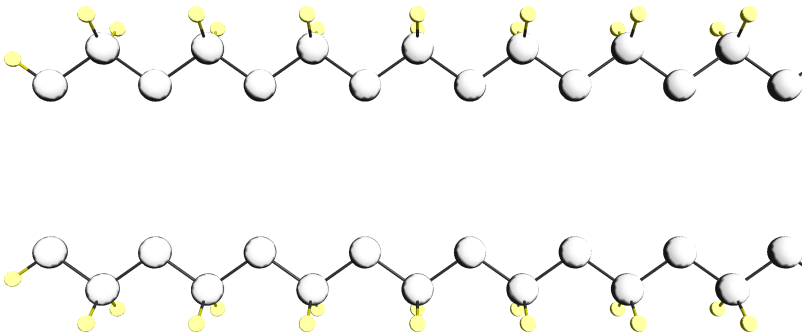

FIG. 5: The $(:C)_8$ dimer. This image was made with MacMolPlt.[97]

specifically, we will investigate $HC(\text{-}CH_2\text{-}C\text{-})_{n-1}H$ for increasing n. Note that each molecule has n carbene sites, and accordingly we will use the notation $(:C)_n$ to denote these molecules. In each molecule, we fixed all C-C bonds at 1.54 Å, all C-H bonds at 1.1 Å, and all angles at 109.5 degrees. The geometries may also be obtained by taking a linear alkane and converting (by H-atom removal) the first, third, fifth, etc. C atoms to carbene sites. There is more than one way to remove two H atoms each from the first and last C atoms. We chose to retain the H atoms furthest from the center of the molecule, thus preserving the C_{2v} symmetry of the molecule's alkane counterpart. For this, one plane contains all the C atoms and the two terminal H atoms, and it bisects the internal H atoms (see the depiction of $(:C)_8$ in the dimer shown in Fig. 5).

We begin by benchmarking CCVB with CASSCF on $(:C)_2$ and $(:C)_4$. In these and all other polycarbene calculations discussed here, we used the cc-pVDZ basis and an active space consisting only of the radical electrons and a matching number of orbitals, which is $(2n, 2n)$ for $(:C)_n$. As done in the preceding subsections, we compute the lowest-energy states for each of the possible spin values consistent with the selected active space. For $(:C)_n$, these would be $s = 0, 1, \ldots, n$. Afterwards we consider longer carbenes, which prove to be computationally problematical, before concentrating on the $(:C)_8$ dimer shown in Fig. 5.

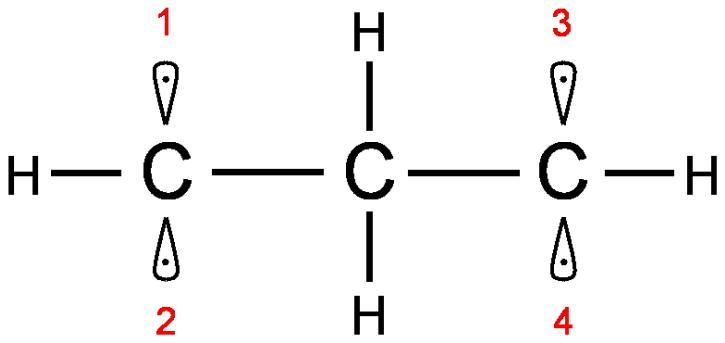

FIG. 6: Ordering used for the localized-orbital guess and to label the unrestricted solutions for $(:C)_2$.

1. *(:C)$_2$*

We started by computing UHF solutions for $(:C)_2$, obtaining them as follows. We first did an $s_z = 2$ ROHF calculation and then localized the four singly occupied orbitals with the Boys procedure.[98] This resulted in four sp^3 hybridized atomic-like orbitals, with two on each carbene carbon atom. These orbitals point along the directions of the "missing" C-H bonds, i.e. those present in the counterpart linear alkane. For the purposes of description, we order the orbitals as shown in Fig. 6.

To obtain initial guesses for UHF, we can assign four spins $\sigma_1, \sigma_2, \sigma_3, \sigma_4$ to the ordered localized orbitals, and for later usage, we will denote such assignments by $(\sigma_1\sigma_2)$-$(\sigma_3\sigma_4)$, where we have included the parentheses and dash to separate the carbene sites. We will use the same notation to label the UHF solutions resulting from these guesses. Assigning the spins in all possible unique ways, we obtain several solutions, the lowest of which for each s_z value are given in Table I. Note that all HF and DFT solutions presented in this subsection were shown to be internally stable using stability analysis. We see that, according to UHF, CH_2 is a fCU for this system. This is corroborated by frozen-core CCSD(T) calculations based on these UHF solutions, whose energies are also shown in Table I.

As done in the previous subsections, we used the orbitals from the lowest $s_z = 0$ UHF solution as input to a singlet CCVB calculation, then used the results of the latter as inputs for the CCVB triplet and quintet calculations. The energies of these calculations are included in Table I. Also included are CASSCF energies for these states. These were obtained using

TABLE I: $(:C)_2$ energies (a.u.).

s	CCVB	CASSCF	MRMP2	UHF	UCCSD(T)	UB3LYP
0	-115.708776	-115.708777	-116.041951	-115.717702	-116.083853	-116.429349
1	-115.709585	-115.709615	-116.043065	-115.708584	-116.083588	-116.424507
2	-115.711695	-115.711695	-116.045644	-115.720846	-116.086412	-116.418890

an Extended-Huckel-Theory guess for the orbitals as implemented in GAMESS. We see that CCVB is in good agreement with CASSCF and that these two models also assert that CH_2 is a fCU for this system. This is corroborated by frozen-core (state-specific) multireference MP2 (MRMP2)[99,100] calculations based on these CASSCF solutions, as shown in Table I.

We also performed DFT calculations on this system, using the same initial-guess strategy used for UHF. We began with B3LYP,[101] whose results are shown in Table I. For these and all other DFT calculations reported in this subsection, the SG-0 grid[102] was used. For UB3LYP, the energy order of the states is opposite to that of the ab initio methods. To investigate this, we need to describe the various unrestricted solutions in more detail.

For the initial guesses for the $s_z = 1$ case, any assignment of three α spins and one β spin to the orbitals gives a solution equivalent to $(\alpha\alpha)$-$(\alpha\beta)$. The $s_z = 2$ solution is obviously also unique. For the $s_z = 0$ case, there are three energetically distinct ways to assign the spins for the initial guess, so there are three unique UHF or UDFT solutions: $(\alpha\alpha)$-$(\beta\beta)$, $(\alpha\beta)$-$(\alpha\beta)$, and $(\alpha\beta)$-$(\beta\alpha)$. The first of these has local s_z values of 1 and -1 on the two carbene sites, hence it is roughly a triplet-triplet coupling of the two carbenes. The other two solutions have local s_z values of 0 on each site, so they each may be viewed as coupling two (broken-symmetry) singlet carbenes. The HF and B3LYP energies for these solutions are given in Table II. We see that UHF clearly favors triplet carbene sites, in line with its assignment of the quintet as the ground state. This explains the poor accuracy of the UHF $s_z = 1$ energy, whose solution treats one carbene with a broken symmetry singlet. CCSD(T) is able to partially correct this, but the basic problem persists. Also included in Table II are the results of frozen-core CCSD(T) calculations based on the pertinent UHF solutions. This higher level of theory significantly closes the gap between the $(\alpha\alpha)$-$(\beta\beta)$ state and the others, but the former remains the lowest in energy.

Because the $(\alpha\alpha)$-$(\beta\beta)$ solution was used to obtain the lowest CCVB singlet, the latter

TABLE II: Energies (a.u.) of the $(:C)_2$ $s_z = 0$ unrestricted solutions.

solution	CCVB	UHF	UCCSD(T)	UB3LYP	UBLYP	UωB97X
$(\alpha\alpha)$-$(\beta\beta)$	-115.708776	-115.717702	-116.083853	-116.417183	-116.349678	-116.380993
$(\alpha\beta)$-$(\alpha\beta)$	-115.692979	-115.697141	-116.080874	-116.429273	-116.364489	-116.389231
$(\alpha\beta)$-$(\beta\alpha)$	-115.692744	-115.696719	-116.080562	-116.429349	-116.364805	-116.389166

also is a coupling of two triplet carbenes, and the same may be said of the CASSCF singlet. Indeed, significantly higher energies result if the other $s_z = 0$ solutions are used for initial guesses in CCVB, as shown in Table II. We have labelled these solutions in accordance with their UHF counterparts, although in CCVB, no orbital is tied to any one spin. We note that the carbene orbitals for the $(\alpha\beta)$-$(\alpha\beta)$ and $(\alpha\beta)$-$(\beta\alpha)$ solutions in UHF and UDFT break symmetry by mixing σ and π, while this is not true for the $(\alpha\alpha)$-$(\beta\beta)$ solutions.

For the lowest CCVB singlet, the most polarized pair contains two π orbitals, one localized to each carbene site, with a similar situation occurring with sp^2 hybridized σ orbitals in the other pair. This inter-carbene pairing structure is intuitive; an intra-carbene structure would correspond to the coupling of two singlet carbene sites. For singlet CCVB, the pair-pair amplitude is 0.5766, which is near $1/\sqrt{3}$, the maximal value for breaking a covalent bond. For the triplet, the OS orbitals are π, and the CS/OS amplitudes are $\pm$ 0.5748. This electron correlation is what allows CCVB, unlike UHF, to be accurate for the triplet, and this is similar to what was observed above for the intermediate spin states of P_2.

Turning to the $s_z = 0$ UB3LYP solutions, we see that those with broken-symmetry singlet carbene sites are clearly favored by this functional. To check this, we computed the same solutions with two other functionals, BLYP[103,104] (no exact exchange) and ωB97X.[105] The latter uses a Coulomb attenuation parameter of 0.3 bohr^{-1}, and was included to see if a reduction of self-interaction error would have any significant effect on the energy orderings. Table II shows that, although the energy spacings between solutions are sensitive to exact exchange, these functionals also favor singlet carbene sites, with ωB97X preferring the $(\alpha\beta)$-$(\alpha\beta)$ solution. Thus none of the three functionals predicts the same ordering as the wave-function methods.

These DFT results look questionable, but is it possible that they correspond to a singlet state that is an excited state at e.g. the CASSCF level, yet is the ground state in a more fully

TABLE III: CH_2 energies (a.u.).

s	CCVB	FCI	UHF	UB3LYP
0	-38.900706	-39.021891	-38.902486	-39.144726
1	-38.914492	-39.034679	-38.918481	-39.145171

correlated picture? Only the UCCSD(T) results (of those considered so far) have bearing on this point, but their accuracy may be limited by significant spin (and space) contamination. In hopes of settling this HF/DFT discrepancy, we turned to CASSCF. A state-specific calculation for the first excited singlet was unsuccessful due to energy oscillations in the orbital optimization. A state averaged CASSCF calculation based on the first two singlets was successful, giving energies of -115.701910 and -115.682372 Hartree for the two states. Using these states, we performed frozen-core MRMP2 calculations (in the form of Multi-configurational Quasidegenerate Perturbation Theory[106,107]). This gave corrected energies of -116.041640 Hartree for the lowest CASSCF state and -116.029644 Hartree for the excited CASSCF state. So, like the above UCCSD(T) results, the more complete correlation treatment causes the gap to narrow, but the ordering is preserved.

Unlike the singlet ground state, the excited state is not strongly correlated, having, at the CASSCF level, a coefficient of 0.930544 on the determinant in which both active sigma orbitals are doubly occupied. This is reminiscent of the electronic structure of the low lying states of CH_2, methylene, which has a triplet ground state and an essentially non-radicaloid lowest singlet. The latter state is dominated by a restricted-orbital determinant in which the carbene σ orbital is doubly occupied and there is no π occupation. For completeness, we include the results of (2,2) CCVB, RHF-based frozen-core FCI, UHF, and UB3LYP calculations on methylene in Table III, with a bond length of 1.09 Å and an angle of 110°. Compared to FCI, CCVB gives an accurate singlet-triplet gap, while UHF is also fairly good in this regard. Yet the analogous solutions in UB3LYP produce a significantly different result, with the $s_z = 1$ energy only narrowly being the lowest.

The methylene example thus affords us two parallels: the lowest $s_z = 0$ UB3LYP solutions for $(:C)_1$ and $(:C)_2$ are analogues, and the lowest singlet of $(:C)_1$ and (ab initio) first excited singlet of $(:C)_2$ are analogues. In methylene, the $s_z = 0$ UB3LYP solution is clearly problematic as an approximation to the lowest singlet state, and this suggests that in $(:C)_2$,

TABLE IV: $(:C)_4$ energies (a.u.).

s	CCVB	CASSCF	MRMP2	UHF
0	-269.303530	-269.303611	-270.100832	-269.322203
1	-269.303687	-269.303924	-270.101266	-269.315842
2	-269.304031	-269.304456	-270.101923	-269.321806
3	-269.304948	-269.305045	-270.102582	-269.315688
4	-269.305631	-269.305631	-270.103201	-269.324640

the lowest $s_z = 0$ UB3LYP solution is problematic as an approximation to the (ab initio) first excited singlet state. It should not be viewed as an approximation to the triplet-triplet coupled singlet or to the quintet, because, among other reasons, both the $(\alpha\alpha)$-$(\beta\beta)$ and $(\alpha\alpha)$-$(\alpha\alpha)$ solutions are higher in energy. Thus, the lowest UB3LYP solution does not match up with any one low lying state, and perhaps it is best viewed as a mixture of several states that has an erroneously low energy.

2. (:C)$_4$

In the $(:C)_4$ calculations, we followed a strategy similar to that used above for $(:C)_2$. We first obtained UHF solutions for different s_z values. We then used the best $s_z = 0$ solution as input to a CCVB singlet calculation, and then used the results of the latter to generate a CCVB spin series. Using the Huckel orbital guess, state specific CASSCF and MRMP2 calculations were performed for the pertinent spin states.

The energies of the lowest-energy UHF solutions for each spin value are given in Table IV. Once again, UHF has clear inaccuracies for the intermediate spin states. This does not occur in the CCVB results, which may be found in Table IV along with the pertinent CASSCF and MRMP2 data. We see that CCVB provides a good approximation to CASSCF here. Again, this is achieved through significant electron correlation, and indeed every CCVB amplitude for each spin state is large, despite the fact that each orbital is fairly well localized. We will look at this type of behavior in more depth in later sub-subsections.

We also attempted to find the lowest-energy UB3LYP solutions for $(:C)_4$. We computed the $(\alpha\alpha)$-$(\alpha\alpha)$-$(\beta\beta)$-$(\beta\beta)$ and $(\alpha\alpha)$-$(\alpha\alpha)$-$(\alpha\alpha)$-$(\alpha\alpha)$ solutions, i.e. those corresponding to the

TABLE V: Energies (a.u.) of the $(:C)_4$ UB3LYP solutions.

Solution	Energy
$(\alpha\alpha)$-$(\alpha\alpha)$-$(\beta\beta)$-$(\beta\beta)$	-270.9618978981
$(\alpha\alpha)$-$(\alpha\alpha)$-$(\alpha\alpha)$-$(\alpha\alpha)$	-270.9629643654
$(\alpha\beta)$-$(\alpha\beta)$-$(\alpha\beta)$-$(\alpha\beta)$	-270.9937959464
$(\alpha\beta)$-$(\alpha\beta)$-$(\alpha\beta)$-$(\beta\alpha)$	-270.9937807582
$(\alpha\beta)$-$(\alpha\beta)$-$(\beta\alpha)$-$(\alpha\beta)$	-270.9934547752
$(\alpha\beta)$-$(\alpha\beta)$-$(\beta\alpha)$-$(\beta\alpha)$	-270.9938636065
$(\alpha\beta)$-$(\beta\alpha)$-$(\alpha\beta)$-$(\beta\alpha)$	-270.9930417958
$(\alpha\beta)$-$(\beta\alpha)$-$(\beta\alpha)$-$(\alpha\beta)$	-270.9937676764

lowest $s_z = 0$ and $s_z = 4$ UHF solutions, and show their energies in Table V. Relative to one another, they behave similarly to their UHF counterparts. However, we again found that B3LYP clearly favors placing local $s_z = 0$ values on the carbene sites. There are 6 energetically unique ways of placing one α and one β spin at each carbene site, and since it was not intuitive to us which one would be lowest in energy, we computed them all and have included the results in Table V. As was the case for $(:C)_2$, we are inclined to think that none of these local $s_z = 0$ solutions is a meaningful approximation to any particular exact state, and the subtle energetic differences between them only seem to increase the ambiguity of the performance of UB3LYP for these systems.

3. Larger $(:C)_n$

We attempted to calculate spin-state series for longer polycarbene chains, i.e. $(:C)_8$, $(:C)_{12}$, $(:C)_{16}$, and $(:C)_{20}$. For these calculations, the computation time was greatly shortened by using the resolution of the identity (RI) approximation.[108–110] The rimp2-cc-pVDZ auxiliary basis[111] and pure basis functions were employed in all calculations reported in this and the following sub-subsection.

Several numerical difficulties were encountered in these calculations, and we were unable to obtain proper CCVB solutions for many of the spin states of these larger molecules. We describe and discuss this situation at length in the Supplementary Information, where we

conclude that these difficulties originate from a subtle interplay between sparsity in the off-diagonal Hamiltonian matrix elements and small gaps in the diagonal elements. For these polycarbenes, the outcome of this interplay is that *all* the CCVB amplitudes are large, even when using highly localized orbitals. We will be able to further analyze this curious phenomenon in the next sub-subsection.

We essentially have two options for proceeding with polycarbene calculations. We could continue to pursue the $(:C)_n$ molecules by attempting to improve our numerical approaches, or we could modify the geometrical aspects of these systems. We chose the latter route, having been influenced by the following viewpoint: the singlet ground state of a long $(:C)_n$ with n even may be viewed roughly a $s = n/2$ polycarbene (the "left" half of the molecule) coupled to another $s = n/2$ polycarbene (the "right" half) to form a low overall spin. These conceptual subunits meet end to end, but we observed that when the geometries of these polycarbenes are optimized in the highest spin state, the molecules curve into an arc-like shape. Thus, the interaction between the subunits increases and the energy gaps slightly increase. Some moderate improvements in the numerical problems were observed when we tried using such optimized geometries in spin-state series calculations. This contributed to the idea that the side-by-side interaction of two high-spin linear polycarbenes might well present with less numerical difficulties, while also being more physically interesting than the end-to-end interaction because it serves as a model for how these molecules might interact in the condensed phase. Accordingly, we switched our focus to a $(:C)_8$ dimer.

4. $(:C)_8$ dimer

We will consider geometries in which each carbene site of one monomer faces its counterpart of the other monomer, with each of these carbene-carbene lengths being the same. This is the interaction of a $(:C)_8$ monomer with its "mirror image", and is depicted for one inter monomer distance in Fig. 5. As the monomers are brought closer and closer together, each carbene forms an ethylene-like double bond with its mirror counterpart, with the system eventually becoming a chain of fused 1,4-cyclohexadiene units. We will apply both the UHF guess (UG) and a "fully localized guess" (FLG). For the latter, each sp^2-hybrid σ orbital of each carbene carbon is paired with its counterpart on the other monomer, and the π orbitals are paired similarly. Once again, the active space consists of the radical electrons, i.e. it is

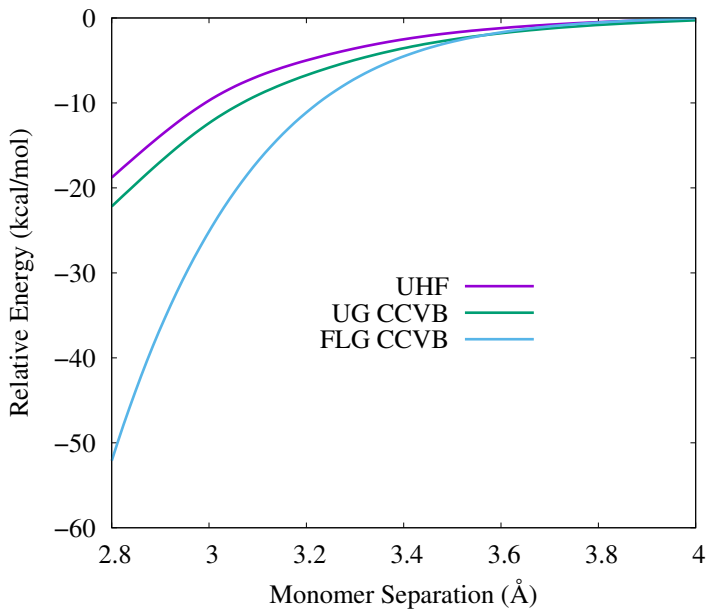

FIG. 7: $(:C)_8$ dimer singlet PES. FLG CCVB used fully localized guess (FLG) orbitals, and UG CCVB used the UHF guess (UG) and has highly delocalized orbitals. UHF energies are relative to two times the $s_z = 8$ UHF energy of the monomer, and CCVB energies are relative to the $s = 16$ ROHF energy at 50 Å monomer separation.

(32,32).

For the singlet, the UG and FLG results are shown along with those of $s_z = 0$ UHF in Fig. 7. For UHF, the energies are relative to two times the $s_z = 8$ UHF energies for the monomer, while for CCVB, the energies are relative to the $s_z = 16$ ROHF energy of the dimer at 50 Å separation. Both CCVB curves dissociate to the correct limit. They cross between 3.4 and 3.6 Å; to the right of this point, the UG curve is slightly lower than the FLG one, while to the left, FLG becomes lower by a rather large gap. This is because the UG results have highly delocalized orbitals, which are unsuited to reduced coupled cluster models like CCVB.

Further insight may be gained by noting that the PUHF and CCVB wave functions have the same basic coupled-cluster form, as proved in ref. 59. Thus, given the same orbitals and pair polarization angles, the difference between the PUHF and CCVB wave functions lies solely in the values of the t_{ka} amplitudes. At 3 Å monomer separation, the smallest and largest UG CCVB amplitudes are 0.49696 and 0.57565 respectively, while the amplitudes with the same pair indices of the PUHF wave function are 0.50028 and 0.57568, and in that

case these are again the smallest and largest amplitudes. The other amplitudes similarly match up, and this agreement is also observed at the other geometries. Therefore, the UG CCVB solution is essentially equivalent to PUHF. PUHF is not size extensive and in particular its correlation energy with respect to UHF scales sublinearly. This is consistent with the UG CCVB results, which show little improvement over the associated UHF energies.

Continuing to look at the PUHF wavefunction in terms of CCVB configurations, we can understand its size extensivity failure and how CCVB overcomes this, as demonstrated by the FLG solution for the $(:C)_8$ dimer. Eqns. (A84) and (A91) of ref. 59 show that the PUHF t_{kl} amplitudes are simple functions of the θ_k, i.e. the pair polarization angles. In particular, the magnitude of a PUHF amplitude is large if the polarizations of the two associated pairs are large, regardless of their relative distance or any other physical characteristics. For example, for the side-by-side interaction of two stretched N_2 molecules (as touched on briefly in the Supplementary Information), the intermolecular PUHF amplitudes are large, and as a result the PUHF energy is not size consistent for that system.

The CCVB amplitude equations are rooted in a projective eigenvalue approximation, so the amplitudes are determined by the physical interactions between the pairs, resulting in size consistency for sufficiently localized orbitals. This is nicely illustrated in the FLG solution. At 3 Å separation, the pairs are significantly polarized: the σ-pair angles are all around 1.34 radians and those for the π-pairs are all around 1.52 radians, while maximal polarization is about 1.57 radians. For these parameters, the PUHF amplitudes would be large and uniform regardless of the distance between these maximally localized pairs. The CCVB situation is quite different as depicted in Fig. 8a. The σ-π amplitude for each stretched double bond is large and there is a rapid magnitude reduction as the distance between pairs increases. These distinctions in amplitude behavior correspond to the large difference between the PUHF curve (as implied by the UG curve) and FLG curve in this region.

For 4 and 5 Å monomer separations, the FLG CCVB amplitude magnitudes are depicted in Figs. 8b and 8c, respectively. We observe a striking increase in pair-correlation length scale as the monomer separation increases. Indeed, near full entanglement is reached by 5 Å separation. The amplitude decay rate as a function of the interpair distance is much slower than that for the corresponding matrix elements. We have arrived at a situation similar to what was found for the low-spin states of a long $(:C)_n$: numerous pairings of small off-

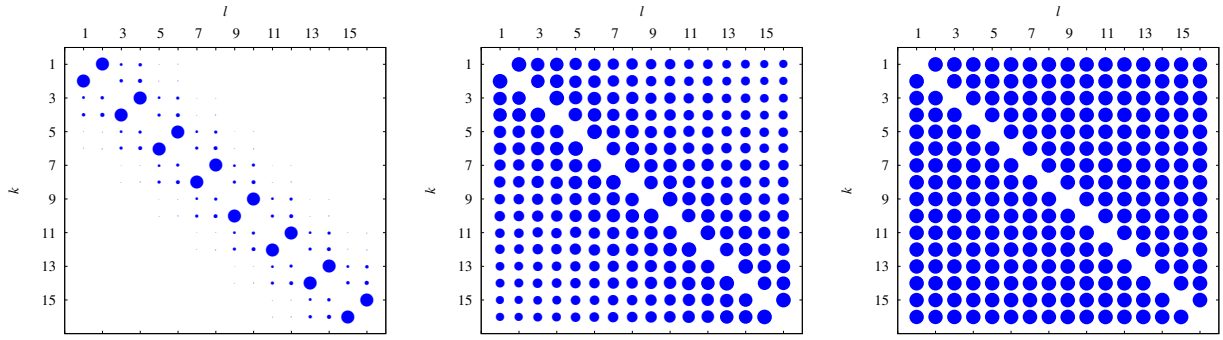

(a) $r = 3$ Å (b) $r = 4$ Å (c) $r = 5$ Å

FIG. 8: Graphical depiction of the matrix of $s = 0$ CCVB t amplitudes for various monomer separations in the $(:C)_8$ dimer. The matrix indices are the pair indices, which increase going from left to right in Fig. 5, i.e. the order of the pairs is 1-σ, 1-π, 2-σ, 2-π, etc., where 1 indicates the leftmost carbene-carbene "column", 2 is for the next column, etc. The size of each blue circle represents the magnitude of that amplitude relative to $1/\sqrt{3}$. For reference, the magnitudes of all the amplitudes for panel (c) are very close to this value.

diagonal matrix elements and small gaps that collectively produce many large amplitudes.

This phenomenon is rarely encountered in chemistry and may even seem dubious, but it can be unambiguously verified. Consider the lowest-energy exact (within the (32,32) active space) states for each spin value. In the limit of infinite monomer separation, the energy of each of these states becomes equal to two times the $s = 8$ ROHF energy for $(:C)_8$. If spin polarization were allowed only within this active space, the corresponding $s_z = 0$ UHF energy would reach the same limit, and therefore the corresponding PUHF wave functions for each spin value would also approach exactness. This UHF wave function becomes a product of two monomer ROHF wave functions, one with 16 net α spins and the other with 16 net β spins. The singly occupied ROHF orbitals may be (orthogonally) localized into quasi-atomic σ and π orbitals, so, from orbital invariance, these may be selected to represent the UHF wave function. Because the α and β spaces localize to separate monomers, they eventually become fully orthogonal to one another. We can imagine pairing these localized UHF orbitals in the same way found in the FLG CCVB solution, and this will become a strongly orthogonal set of pairs in the dissociation limit. With this representation of the

UHF wavefunction, we can apply singlet spin projection in the CCVB fashion, i.e. expanding the resulting wavefunction in terms of CCVB configurations. It is then clear that the FLG CCVB and PUHF wave functions are one and the same in the dissociation limit, meaning FLG CCVB is exact there. Note that this result holds if we change the relative orientation of the monomers, i.e. we consider something other than the mirror-image interaction: as the monomers are pulled apart there will always be this massive increase in long-range correlation.

We now examine the higher spin states of the $(:C)_8$ dimer. Employing the procedure used repeatedly above, we have computed the $s = 0$ through $s = 16$ spin series for a few geometries. The data for 1.8, 2.4, and 3 Å monomer separations are shown in Table VI. As can be seen, the range of the energies at 1.8 Å is much larger than at 3 Å. At each geometry, the π pairs are more polarized than the σ pairs. Thus the $s = 1$ through $s = 8$ calculations are based on converting from 1 to 8 CS π pairs to OS form. As can be seen in Table VI, the energetic penalties for these spin flips, i.e. the difference between the $s = m$ and $s = m + 1$ energies for $m = 0 \ldots 7$, are all roughly the same. The remaining spin states sequentially convert the σ pairs, and the associated spin flip energy penalties are again uniform. However, the energy required to spin-flip a σ pair is larger than that for a π pair.

CCVB is able to properly dissociate each spin state, which is something that UHF would be unable to do for intermediate spin values, i.e. for s_z values from 1 through 15. In the dissociation limit, each spin state exhibits maximal entanglement in both the CS/CS and CS/OS realms. To illustrate, we have depicted the CS/OS amplitudes of the $s = 8$ calculation in Figs. 9a-9c. As implied above, the CS pairs of this CCVB solution comprise all the active σ bonds, while the OS part consists of all the π orbitals. Similar to the singlet case, at 3 Å monomer separation, the only large CS/OS amplitudes are those corresponding to the σ and π interactions within each stretched double bond, with the main difference being that the single amplitude used in the $s = 0$ calculation to describe the correlation of adjacent σ and π electrons has become two amplitudes in the $s = 8$ calculation due to the OS individualization of the pertinent π electrons. Looking at Figs. 9b and 9c, we again see a concerted and dramatic increase in correlation magnitudes with increasing monomer separation.

To further discuss the non-local correlation phenomena uncovered above, consider the "mirror-image" interaction of two $(:C)_1$'s approaching each other until their radical electrons

TABLE VI: CCVB energies for the $(:C)_8$ dimer at various monomer separations. Energies (kcal/mol) are relative to the $s = 16$ ROHF energy at 50 Å monomer separation.

s	$r = 1.8$ Å	$r = 2.4$ Å	$r = 3.0$ Å
0	-751.074	-183.946	-25.120
1	-718.011	-174.146	-22.399
2	-684.948	-164.346	-19.679
3	-650.541	-154.222	-16.975
4	-616.133	-144.099	-14.274
5	-581.865	-134.272	-11.569
6	-547.722	-124.742	-8.879
7	-513.529	-115.212	-6.186
8	-479.336	-105.683	-3.494
9	-305.042	-69.525	1.439
10	-130.748	-33.368	6.372
11	41.428	2.035	11.037
12	213.608	37.438	15.701
13	387.661	73.207	20.035
14	563.275	109.298	24.038
15	739.622	145.522	28.034
16	915.969	181.746	32.030

pair into a double bond and ethylene is formed. For stretched bond lengths, the CCVB amplitude correlating the two pairs of the double bond would grow large. If we consider the simultaneous dissociation of two parallel ethylene molecules separated by a few angstroms, the two CCVB amplitudes correlating the pairs within double bonds would behave as in the single ethylene case, while the amplitudes correlating one pair from each molecule would be very small. The operative detail is that the exchange interaction between the two unpaired electrons of any one $(:C)_1$ is significant, while the exchange interaction between unpaired electrons on different fragments is not.

This exemplifies one of the key general concepts to come out of CCVB theory: in the

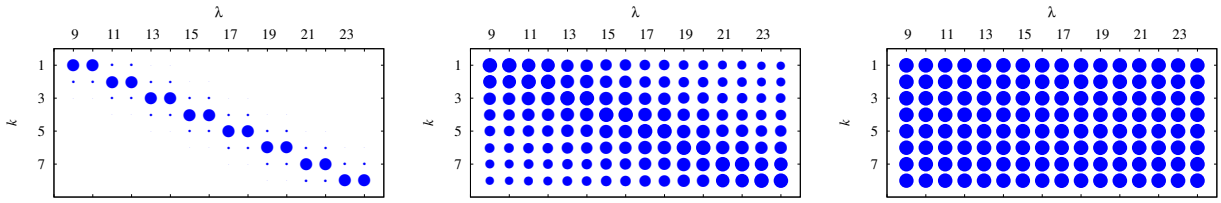

(a) $r = 3$ Å (b) $r = 4$ Å (c) $r = 5$ Å

FIG. 9: Same as for Fig. 8, but for the CS/OS block of the matrix of $s = 8$ CCVB t amplitudes. The CS pairs are all σ, and the OS electrons are all π. These correspond to the rows and columns, respectively, of the matrix, and their orderings are analogous to that listed in Fig. 8.

simultaneous breaking of covalent bonds, the correlation between the bonds is driven largely by exchange interactions on the associated fragments, or put more generally, a significant piece of the *exchange* interactions within fragments assumes the form of *correlation* between electron pairs when such fragments are low-spin coupled. Exchange interactions are the reason that the $s = 8$ state of $(:C)_8$ is the lowest in energy at the (16,16) level, so the preceding concepts indicate that the associated dimer would have at least several large CCVB amplitudes for larger monomer separations. However, exchange interactions diminish rapidly with increasing distance, so it is quite remarkable that electron correlation can so substantially outlast its own impetus. The fact that the exchange interactions are uninterrupted over the length of the monomer is evidently pivotal.

IV. CONCLUSIONS

In this paper, we have developed the CCVB method for open-shell systems. After introducing the basic OS CCVB wavefunction, we described at length how to embed it in a larger singlet supersystem. From this, OS CCVB becomes more theoretically similar to and as computationally feasible as CS CCVB, and can easily be implemented by modifying code for the latter. Thus, as for CS CCVB, the OS CCVB algorithm is dominated by the two-electron integral transformations, which have 5th order scaling, this being reduced to 4th order for larger systems. The primary difference between OS CCVB and CS CCVB is the limited presence of certain 3-pair correlations in the former. We are currently working

on the more general incorporation of these 3-pair correlations into CCVB.

The OS CCVB method was demonstrated for several molecular examples, including P_2, Mn_2^+ and various polycarbenes. It was shown that, like CS CCVB, OS CCVB is able to correctly describe the various spin couplings of high-spin fragments, such as is found in the dissociation of multiple bonds and in polyradicals, thereby exceeding the capabilities of mean-field methods. Every example spotlighted the importance of a proper treatment of CS/OS correlation in strongly correlated systems.

CCVB was used to study the interaction of two long polycarbene chains. Unlike the related PUHF, CCVB has flexibility in its correlation amplitude structure, which allows it to accommodate the electronic structure extremes found in this system: at short range, the system has lightly interacting double bonds of fused cyclohexadiene units, while at long range, massive entanglement over great distances is exhibited. Indeed, in the monomer dissociation limit, the strong correlation is boundless in terms of polycarbene chain length. This characterstic makes this and similar systems objects of interest for future study.

We assert that this paper and its predecessors have shown that CCVB has clear theoretical and computational value. At the same time, CCVB can often be challenging to use in applications. This is primarily because of its electron-pairing framework; a simplification that gives great computational benefits and provides conceptual and interpretational advantages, but is at times simply incompatible with the exact electronic structure. For CS systems, this issue was greatly ameliorated with the introduction of the CCVB-SD method, wherein amplitudes corresponding to all singles and doubles configurations and higher-order clusters thereof are treated in the CCVB framework. By evaluating the CCVB-SD residual using the CCVB amplitudes and orbitals, we obtain a relatively inexpensive indication of the qualitative accuracy of CCVB results in practice. An analogous generalization of OS CCVB into an OS CCVB-SD method is of significant interest for future work.

SUPPLEMENTARY MATERIAL

Detailed discussion of the computations referred to in Section III C 3.

ACKNOWLEDGMENTS

This work was supported by the Director, Office of Science, Office of Basic Energy Sciences, of the U.S. Department of Energy under Contract No. DE-AC02-05CH11231, with additional support from a subcontract from MURI Grant W911NF-14-1-0359.

[1] W. Kohn, A. D. Becke, and R. G. Parr, J. Phys. Chem. **100**, 12974 (1996).

[2] R. O. Jones, Rev. Mod. Phys. **87**, 897 (2015).

[3] J. Klimes and A. Michaelides, J. Chem. Phys. **137**, 120901 (2012).

[4] J. Calbo, E. Orti, J. C. Sancho-Garcia, and J. Arago, in *Annual Reports in Computational Chemistry, vol. 11*, edited by A. D. David, pp. 37 – 102 (Elsevier, 2015).

[5] N. Mardirossian and M. Head-Gordon, J. Chem. Phys. **144**, 214110 (2016).

[6] A. J. Cohen, P. Mori-Sanchez, and W. T. Yang, Chem. Rev. **112**, 289 (2012).

[7] R. J. Bartlett and M. Musial, Rev. Mod. Phys. **79**, 291 (2007).

[8] D. Cremer, WIREs Comput. Mol. Sci. **1**, 509 (2011).

[9] K. Raghavachari, G. W. Trucks, J. A. Pople, and M. Head-Gordon, Chem. Phys. Lett. **157**, 479 (1989).

[10] D. W. Small and M. Head-Gordon, Phys. Chem. Chem. Phys. **13**, 19285 (2011).

[11] N. J. Mayhall and M. Head-Gordon, J. Chem. Phys. **141**, 134111 (2014).

[12] J. Hachmann, J. J. Dorando, M. Avilés, and G. K.-L. Chan, J. Chem. Phys. **127**, 134309 (2007).

[13] H. F. Bettinger, Pure Appl. Chem. **82**, 905 (2010).

[14] B. O. Roos, P. R. Taylor, and P. E. M. Siegbahn, Adv. Chem. Phys. **48**, 157 (1980).

[15] P. Siegbahn, A. Heiberg, B. Roos, and B. Levy, Physica Scripta **21**, 323 (1980).

[16] P. E. M. Siegbahn, J. Almlöf, A. Heiberg, and B. O. Roos, J. Chem. Phys. **74**, 2384 (1981).

[17] K. Ruedenberg, M. W. Schmidt, M. M. Gilbert, and S. T. Elbert, Chem. Phys. **71**, 41 (1982).

[18] K. Ruedenberg, M. W. Schmidt, and M. M. Gilbert, Chem. Phys. **71**, 51 (1982).

[19] K. Ruedenberg, M. W. Schmidt, M. M. Gilbert, and S. T. Elbert, Chem. Phys. **71**, 65 (1982).

[20] B. O. Roos, Adv. Chem. Phys. **69**, 399 (1987).

[21] M. W. Schmidt and M. S. Gordon, Annu. Rev. Phys. Chem. **49**, 233 (1998).

[22] D. Ghosh, J. Hachmann, T. Yanai, and G. K.-L. Chan, J. Chem. Phys. **128**, 144117 (2008).

[23] G. K. L. Chan and S. Sharma, Annu. Rev. Phys. Chem. **62**, 465 (2011).

[24] G. Li Manni, S. D. Smart, and A. Alavi, J. Chem. Theor. Comput. **12**, 1245 (2016).

[25] P. A. Malmqvist, A. Rendell, and B. O. Roos, J. Phys. Chem. **94**, 5477 (1990).

[26] V. Veryazov, P. A. Malmqvist, and B. O. Roos, Int. J. Quantum Chem. **111**, 3329 (2011).

[27] A. I. Krylov, C. D. Sherrill, E. F. C. Byrd, and M. Head-Gordon, J. Chem. Phys. **109**, 10669 (1998).

[28] T. Van Voorhis and M. Head-Gordon, Chem. Phys. Lett. **330**, 585 (2000).

[29] J. A. Parkhill, K. Lawler, and M. Head-Gordon, J. Chem. Phys. **130**, 084101 (2009).

[30] J. A. Parkhill and M. Head-Gordon, J. Chem. Phys. **133**, 024103 (2010).

[31] S. Lehtola, J. Parkhill, and M. Head-Gordon, J. Chem. Phys. **145**, 134110 (2016).

[32] G. Gidofalvi and D. A. Mazziotti, J. Chem. Phys. **129**, 134108 (2008).

[33] L. Greenman and D. A. Mazziotti, J. Chem. Phys. **130**, 184101 (2009).

[34] J. Fosso-Tande, N. Truong-Son, G. Gidofalvi, and A. E. DePrince, III, J. Chem. Theor. Comput. **12**, 2260 (2016).

[35] D. L. Cooper, J. Gerratt, and M. Raimondi, Int. Rev. Phys. Chem. **7**, 59 (1988).

[36] D. L. Cooper, J. Gerratt, and M. Raimondi, Chem. Rev. **91**, 929 (1991).

[37] J. Gerratt, D. L. Cooper, P. B. Karadakov, and M. Raimondi, Chem. Soc. Rev. **26**, 87 (1997).

[38] P. B. Karadakov, D. L. Cooper, B. J. Duke, and J. Li, J. Phys. Chem. A **116**, 7238 (2012).

[39] J. Olsen, J. Chem. Phys. **143**, 114102 (2015).

[40] A. C. Hurley, J. Lennard-Jones, and J. A. Pople, Proc. R. Soc. A Math. Phys. Eng. Sci. **220**, 446 (1953).

[41] W. A. Goddard and L. B. Harding, Annu. Rev. Phys. Chem. **29**, 363 (1978).

[42] J. Langlois, R. Muller, T. Coley, W. Goddard III, M. Ringnalda, Y. Won, and R. Friesner, J. Chem. Phys. **92**, 7488 (1990).

[43] A. Sodt, G. J. O. Beran, Y. Jung, B. Austin, and M. Head-Gordon, J. Chem. Theory Comput. **2**, 300 (2006).

[44] P. R. Surján, Top. Curr. Chem. **203**, 63 (1999).

[45] V. A. Rassolov, J. Chem. Phys. **117**, 5978 (2002).

[46] V. A. Rassolov and F. Xu, J. Chem. Phys. **127**, 044104 (2007).

[47] E. Neuscamman, Phys. Rev. Lett. **109**, 203001 (2012).

[48] P. A. Limacher, P. W. Ayers, P. A. Johnson, S. De Baerdemacker, D. Van Neck, and P. Bultinck, J. Chem. Theory Comput. **9**, 1394 (2013).

[49] B. A. Cagg and V. A. Rassolov, J. Chem. Phys. **141**, 164112 (2014).

[50] P. Tecmer, K. Boguslawski, P. A. Johnson, P. A. Limacher, M. Chan, T. Verstraelen, and P. W. Ayers, J. Phys. Chem. A **118**, 9058 (2014).

[51] P. Jeszenszki, P. R. Surjan, and A. Szabados, J. Chem. Theor. Comput. **11**, 3096 (2015).

[52] E. Neuscamman, Mol. Phys. **114**, 577 (2016).

[53] P. A. Limacher, J. Chem. Phys. **145**, 194102 (2016).

[54] F. Faglioni and W. A. Goddard, Int. J. Quantum Chem. **73**, 1 (1999).

[55] R. B. Murphy, R. A. Friesner, M. N. Ringnalda, and W. A. Goddard, J. Chem. Phys. **101**, 2986 (1994).

[56] T. Van Voorhis and M. Head-Gordon, Chem. Phys. Lett. **317**, 575 (2000).

[57] T. Van Voorhis and M. Head-Gordon, J. Chem. Phys. **115**, 7814 (2001).

[58] T. Van Voorhis and M. Head-Gordon, J. Chem. Phys. **117**, 9190 (2002).

[59] D. W. Small and M. Head-Gordon, J. Chem. Phys. **130**, 084103 (2009).

[60] D. W. Small, K. V. Lawler, and M. Head-Gordon, J. Chem. Theory Comput. **10**, 2027 (2014).

[61] K. V. Lawler, G. J. O. Beran, and M. Head-Gordon, J. Chem. Phys. **128**, 024107 (2008).

[62] D. W. Small and M. Head-Gordon, J. Chem. Phys. **137**, 114103 (2012).

[63] J. Lee, D. W. Small, E. Epifanovsky, and M. Head-Gordon, J. Chem. Theory Comput. **13**, 602 (2017), pMID: 28072533.

[64] S. A. Alexander and D. J. Klein, J. Am. Chem. Soc. **110**, 3401 (1988).

[65] A. Rajca, Chem. Rev. **94**, 871 (1994).

[66] W. Mizukami, Y. Kurashige, and T. Yanai, J. Chem. Phys. **133**, 091101 (2010).

[67] J. Brabec, K. Bhaskaran-Nair, K. Kowalski, J. Pittner, and H. J. J. van Dam, Chem. Phys. Lett. **542**, 128 (2012).

[68] T. Van Voorhis and M. Head-Gordon, Mol. Phys. **100**, 1713 (2002).

[69] Y. Shao, Z. Gan, E. Epifanovsky, A. T. Gilbert, M. Wormit, J. Kussmann, A. W. Lange, A. Behn, J. Deng, X. Feng, D. Ghosh, M. Goldey, P. R. Horn, L. D. Jacobson, I. Kaliman, R. Z. Khaliullin, T. Kuś, A. Landau, J. Liu, E. I. Proynov, Y. M. Rhee, R. M. Richard, M. A. Rohrdanz, R. P. Steele, E. J. Sundstrom, H. L. Woodcock, P. M. Zimmerman, D. Zuev, B. Albrecht, E. Alguire, B. Austin, G. J. O. Beran, Y. A. Bernard, E. Berquist, K. Brandhorst, K. B. Bravaya, S. T. Brown, D. Casanova, C.-M. Chang, Y. Chen, S. H. Chien, K. D. Closser, D. L. Crittenden, M. Diedenhofen, R. A. DiStasio, H. Do, A. D. Dutoi, R. G. Edgar, S. Fatehi, L. Fusti-Molnar, A. Ghysels, A. Golubeva-Zadorozhnaya, J. Gomes, M. W. Hanson-Heine, P. H. Harbach, A. W. Hauser, E. G. Hohenstein, Z. C. Holden, T.-C. Jagau, H. Ji, B. Kaduk, K. Khistyaev, J. Kim, J. Kim, R. A. King, P. Klunzinger, D. Kosenkov, T. Kowalczyk, C. M.

Krauter, K. U. Lao, A. Laurent, K. V. Lawler, S. V. Levchenko, C. Y. Lin, F. Liu, E. Livshits, R. C. Lochan, A. Luenser, P. Manohar, S. F. Manzer, S.-P. Mao, N. Mardirossian, A. V. Marenich, S. A. Maurer, N. J. Mayhall, E. Neuscamman, C. M. Oana, R. Olivares-Amaya, D. P. O'Neill, J. A. Parkhill, T. M. Perrine, R. Peverati, A. Prociuk, D. R. Rehn, E. Rosta, N. J. Russ, S. M. Sharada, S. Sharma, D. W. Small, A. Sodt, T. Stein, D. Stück, Y.-C. Su, A. J. Thom, T. Tsuchimochi, V. Vanovschi, L. Vogt, O. Vydrov, T. Wang, M. A. Watson, J. Wenzel, A. White, C. F. Williams, J. Yang, S. Yeganeh, S. R. Yost, Z.-Q. You, I. Y. Zhang, X. Zhang, Y. Zhao, B. R. Brooks, G. K. Chan, D. M. Chipman, C. J. Cramer, W. A. Goddard, M. S. Gordon, W. J. Hehre, A. Klamt, H. F. Schaefer, M. W. Schmidt, C. D. Sherrill, D. G. Truhlar, A. Warshel, X. Xu, A. Aspuru-Guzik, R. Baer, A. T. Bell, N. A. Besley, J.-D. Chai, A. Dreuw, B. D. Dunietz, T. R. Furlani, S. R. Gwaltney, C.-P. Hsu, Y. Jung, J. Kong, D. S. Lambrecht, W. Liang, C. Ochsenfeld, V. A. Rassolov, L. V. Slipchenko, J. E. Subotnik, T. Van Voorhis, J. M. Herbert, A. I. Krylov, P. M. Gill, and M. Head-Gordon, Mol. Phys. **113**, 184 (2015).

[70] M. W. Schmidt, K. K. Baldridge, J. A. Boatz, S. T. Elbert, M. S. Gordon, J. H. Jensen, S. Koseki, N. Matsunaga, K. A. Nguyen, S. J. Su, T. L. Windus, M. Dupuis, and J. A. Montgomery, J. Comput. Chem. **14**, 1347 (1993).

[71] D. Feller, J. Comp. Chem. **17**, 1571 (1996).

[72] K. L. Schuchardt, B. T. Didier, T. Elsethagen, L. Sun, V. Gurumoorthi, J. Chase, J. Li, and T. L. Windus, J. Chem. Inf. Model. **47**, 1045 (2007).

[73] T. H. Dunning, J. Chem. Phys. **90**, 1007 (1989).

[74] A. J. H. Wachters, J. Chem. Phys. **52**, 1033 (1970).

[75] A. J. H. Wachters, IBM Tech. Rept. RJ584 (1969).

[76] C. W. Bauschlicher, Jr., S. R. Langhoff, and L. A. Barnes, J. Chem. Phys. **91**, 2399 (1989).

[77] S. Yamanaka, K. Kanda, T. Saito, Y. Kitagawa, T. Kawakami, M. Ehara, M. Okumura, H. Nakamura, and K. Yamaguchi, Chem. Phys. Lett. **519-520**, 134 (2012).

[78] R. J. Vanzee and W. Weltner, J. Chem. Phys. **89**, 4444 (1988).

[79] A. Terasaki, A. Matsushita, K. Tono, R. T. Yadav, T. M. Briere, and T. Kondow, J. Chem. Phys. **114**, 9367 (2001).

[80] V. Zamudio-Bayer, K. Hirsch, A. Langenberg, M. Kossick, A. Lawicki, A. Terasaki, B. von Issendorff, and J. T. Lau, J. Chem. Phys. **142**, 234301 (2015).

[81] B. W. Wang and Z. D. Chen, J. Chem. Phys. **123**, 134306 (2005).

[82] M. Barborini, J. Phys. Chem. A **120**, 1716 (2016).

[83] M. F. Jarrold, A. J. Illies, and M. T. Bowers, J. Am. Chem. Soc. **107**, 7339 (1985).

[84] D. A. Dougherty, Acc. Chem. Res. **24**, 88 (1991).

[85] H. Iwamura and N. Koga, Acc. Chem. Res. **26**, 346 (1993).

[86] K. Itoh, Chem. Phys. Lett. **1**, 235 (1967).

[87] E. Wasserman, R. W. Murray, W. A. Yager, A. M. Trozzolo, and G. Smolinsky, J. Am. Chem. Soc. **89**, 5076 (1967).

[88] Y. Teki, T. Takui, K. Itoh, H. Iwamura, and K. Kobayashi, J. Am. Chem. Soc. **105**, 3722 (1983).

[89] T. Sugawara, S. Bandow, K. Kimura, H. Iwamura, and K. Itoh, J. Am. Chem. Soc. **106**, 6449 (1984).

[90] T. Sugawara, S. Bandow, K. Kimura, H. Iwamura, and K. Itoh, J. Am. Chem. Soc. **108**, 368 (1986).

[91] Y. Teki, T. Takui, K. Itoh, H. Iwamura, and K. Kobayashi, J. Am. Chem. Soc. **108**, 2147 (1986), pMID: 22175552.

[92] I. Fujita, Y. Teki, T. Takui, T. Kinoshita, K. Itoh, F. Miko, Y. Sawaki, H. Iwamura, A. Izuoka, and T. Sugawara, J. Am. Chem. Soc. **112**, 4074 (1990).

[93] M. Mitani, H. Mori, Y. Takano, D. Yamaki, Y. Yoshioka, and K. Yamaguchi, J. Chem. Phys. **113**, 4035 (2000).

[94] T. Itoh, K. Hirai, and H. Tornioka, Bull. Chem. Soc. Jpn. **80**, 138 (2007).

[95] D. Casanova and M. Head-Gordon, Phys. Chem. Chem. Phys. **11**, 9779 (2009).

[96] F. Bell, P. M. Zimmerman, D. Casanova, M. Goldey, and M. Head-Gordon, Phys. Chem. Chem. Phys. **15**, 358 (2013).

[97] B. M. Bode and M. S. Gordon, J. Mol. Graph. Model. **16**, 133 (1998).

[98] J. M. Foster and S. F. Boys, Rev. Mod. Phys. **32**, 300 (1960).

[99] K. Hirao, Chem. Phys. Lett. **190**, 374 (1992).

[100] K. Hirao, Chem. Phys. Lett. **196**, 397 (1992).

[101] A. D. Becke, J. Chem. Phys. **98**, 5648 (1993).

[102] S. Chien and P. Gill, J. Comput. Chem. **27**, 730 (2006).

[103] A. D. Becke, Phys. Rev. A **38**, 3098 (1988).

[104] C. Lee, W. Yang, and R. G. Parr, Phys. Rev. B **37**, 785 (1988).

[105] J. D. Chai and M. Head-Gordon, J. Chem. Phys. **128**, 084106 (2008).

[106] H. Nakano, J. Chem. Phys. **99**, 7983 (1993).

[107] H. Nakano, R. Uchiyama, and K. Hirao, J. Comp. Chem. **23**, 1166 (2002).

[108] M. Feyereisen, G. Fitzgerald, and A. Komornicki, Chem. Phys. Lett. **208**, 359 (1993).

[109] F. Weigend, M. Häser, H. Patzelt, and R. Ahlrichs, Chem. Phys. Lett. **294**, 143 (1998).

[110] B. I. Dunlap, Phys. Chem. Chem. Phys. **2**, 2113 (2000).

[111] F. Weigend, A. Köhn, and C. Hättig, J. Chem. Phys. **116**, 3175 (2002).